9-27-2010

Measuring Venous Oxygen Saturation Using the Photoplethysmograph Waveform

Zachary Walton

MEASURING VENOUS OXYGENATION USING THE PHOTOPLETHYSMOGRAPH WAVEFORM

A Thesis Submitted to the

Yale University School of Medicine

in Partial Fulfillment of the Requirements for the

Degree of Doctor of Medicine

by

Zachary Doyle Walton

2010

MEASURING VENOUS OXYGENATION USING THE PHOTOPLETHYSMOGRAPHIC WAVEFORM. Zachary D. Walton (Sponsored by Kirk H. Shelley). Department of Anesthesiology, Yale University, School of Medicine, New Haven, CT.

The pulse oximeter measures the arterial oxygen saturation. It accomplishes this through the use of the photoplethysmograph waveform (PPG) at two or more wavelengths. It has been recognized for some time that the movement of venous blood can be detected using the PPG. We hypothesize that the PPG waveform, obtained non-invasively by modern pulse oximeters, can be analyzed via digital signal processing to infer the venous oxygen saturation.

Fundamental to the successful isolation of the venous saturation is the identification of PPG characteristics that are unique to the peripheral venous system. Two such characteristics have been identified. First, the peripheral venous waveform tends to reflect atrial contraction (*e.g.*, a-c-v waveform). Second, ventilation tends to move venous blood preferentially due to the low pressure and high compliance of the venous system.

Red (660nm) and IR (940nm) PPG waveforms were collected from 10 cardiac surgery patients using an esophageal PPG probe. These waveforms were analyzed using algorithms written in Mathematica (Wolfram Research). The eight saturation algorithms (ArtSat, VenSat, ArtInstSat, VenInstSat, RespDC, RespAC, Cardiac, and Harmonic) were applied to the data set. Three of the methods (VenSat, VenInstSat, and RespDC) demonstrate significance difference from ArtSat using the Wilcoxon signed-rank test with Bonferroni correction (p¡0.0071).

This thesis introduces new methods of PPG analysis. Three methods of analysis (VenSat, VenInstSat, and RespDC) succeed in detecting lower saturation blood. The next step is to confirm the accuracy of the measurement by comparing them to a gold standard (*i.e.*, venous blood gas).

ACKNOWLEDGMENTS

I would like to thank Panayiotis A. Kyriacou and his coworkers at the City University, London, UK, for their generosity in sharing their data. This thesis represents a continuation of the investigations performed by the research group led by Dr. Kirk H. Shelley and Dr. David G. Silverman at the Yale University Department of Anesthesiology. In particular, I am deeply indebted to Dr. Shelley for his careful and expert guidance of this work.

Contents

1. Introduction

1.1 Photoplethysmography (PPG)

Photoplethysmography (PPG) entails the *in vivo* sampling of the optical properties of a biological system in order to make inferences about the underlying physiology [1, 2]. This technique is the sensing modality employed by modern pulse oximeters. Several factors have conspired to make these devices ubiquitous. First, the measurement that they provide (oxygen saturation of perfusing blood) conveys critical information about the subject's oxygenation status. Second, these devices obtain this information continuously and non-invasively. Third, advances in algorithms, microprocessors, and optoelectronics have led to cost reductions and performance improvements characteristic of semiconductor-based technologies. The pulse oximeter was identified by the American Society of Anesthesiology (ASA) as a standard operating room monitor in 1990. Furthermore, state law in Massachusetts, New York, and New Jersey mandates that pulse oximeters must be employed before the commencement of sedation or anesthesia.

The PPG waveform has been shown to convey information about a wide range of physiological parameters: heart rate, oxygen saturation, vascular tone, blood pressure, cardiac output, respiration, and volume-status [2]. It is unfortunate that despite this wealth of potentially valuable information contained in the PPG waveform, the

vast majority of PPG-based pulse oximeters provide care providers with only heart rate and oxygen saturation [3, 4]. It is true that most pulse oximeters also display a filtered version of the raw PPG waveform; however, it is currently left to the clinician to make qualitative assessments of underlying physiology using this graphical information. In this work, we will address the measurement of oxygen saturation of venous and arterial blood using the PPG waveform.

1.2 Clinical Utility of Venous Oxygen Saturation ($\mathbf{SvO_2}$)

Conventional pulse oximeters provide real-time information concerning the oxygen saturation of arterial blood (SaO_2). This information indicates how well the body is delivering oxygen to the tissues. However, in order to assess the sufficiency of oxygen delivery, it is useful to know the oxygen consumption as well. For example, early goal-directed therapy, which includes treatment goals for mixed venous saturation (SvO_2), increases survival in septic patients [5].

We can relate oxygen consumption (VO_2), oxygen saturation of arterial blood (SaO_2), oxygen saturation of venous blood (SvO_2), cardiac output (CO), hemoglobin concentration (Hgb), and oxygen-carrying capacity of saturated hemoglobin (k) using the following modified Fick equation:

$$VO_2 = k \times CO \times Hgb \times (SaO_2 - SvO_2). \tag{1.1}$$

Depending on which of these parameters are known, SvO_2 can provide valuable information regarding the remaining parameters. For example, in healthy patients, VO_2 and Hgb are stable, in which case changes in SvO_2 reflect changes in CO. Furthermore, it has been shown that the oxygen gradient (SaO_2-SvO_2) is a useful measurement for

monitoring heart failure [6] and sepsis [7].

The conventional method for continuous monitoring of SvO_2 requires the placement of a catheter in either the superior vena cava or the pulmonary artery. Both of these procedures expose the patient to risk, with complications including pneumothorax, large vein thrombosis, and cardiac arrhythmia [8]. Thus, a non-invasive, continuous method of monitoring SvO_2 would have clear advantages over existing techniques.

The PPG-based methods explored in this thesis are non-invasive in the sense that the probe is not located in the vasculature, but rather at the tissue surface of an accessible part of the body (*e.g.*, the finger, the ear, the forehead, the esophagus). SvO_2 is, by definition, the oxygen saturation of the blood that results from the mixing of the venous output from all the tissues of the body. Since many of factors that influence venous oxygen saturation are subject to regional control, one should not expect a given peripheral venous oxygen saturation to mirror SvO_2. Nonetheless, the results presented in Ref. [9] suggest that peripheral venous oxygen saturation at the finger may have clinical relevance on par with SvO_2. For example, it is shown that this peripheral saturation can allow detection of changes in CO and VO_2 in a variety of physiological and pathological conditions.

1.3 History of Photoplethysmography

Plethysmography is a general term describing the study of change in a physical parameter such as volume or optical absorbance in a localized region of tissue. In photoplethysmography (PPG), a light source is placed against a region of tissue, and a light detector is placed either adjacent to the source (*i.e.*, reflection mode, for example at the forehead) or on the other side of the tissue (*i.e.*, transmission mode,

for example at the finger). The PPG waveform is derived from the light intensity recorded by the detector, and typically depends on many factors, including the time-varying engorgement of blood in the region of interest. Prior to the development of the photoplethysmograph, plethysmography was performed via a mechanical strain gauge wrapped around the limb of interest.

In 1936, two research groups (Molitor and Kniazuk of the Merck Institute of Therapeutic Research, New Jersey, and Hanzlik *et al* of Stanford University School of Medicine) reported the first photoplethysmographic instruments, employed to monitor blood volume changes in the rabbit ear following venous occlusion and with administration of vasoactive drugs [10]. In 1937, Alrick Hertzman from the Department of Physiology at St. Louis University School of Medicine reported the use of a photoplethysmograph to measure blood volume changes in the fingers of healthy subjects undergoing the Valsalva maneuver, exercise, and cold exposure [11, 12]. Shortly afterwards, Hertzman and coworkers published a validation study demonstrating close agreement between the photoplethysmograph and the mechanical plethysmograph [13]. Long before the discovery of pulse oximetry, the photoplethysmograph was recognized for its utility in several clinical settings. For example, the PPG waveform provides characteristic responses to cardiovascular shock [14], sedation [15], and changes in vascular sympathetic tone [16, 17].

Early developers of photoplethysmography faced several technical challenges. Among the desirable properties of the plethysmograph light source are: small size, high efficiency, low temperature, stable intensity, narrow-band frequency output. The battery-powered torch bulb used in the pioneering work by Hertzman *et al.* fell far short of the ideal light source. The development of semiconductor technology has led to improvements in the light source, along with nearly every other component of the photoplethysmograph. Light emitting diodes (LED), photodiodes, and digital

signal processing are among the numerous technological advances that have led to radical improvements in the performance of modern photoplethysmographs. It was serendipitous that while the technology underlying photoplethysmography was riding the microelectronics boom, a method was discovered for using this sensing modality to measure the oxygen saturation of blood perfusing a given body part [18, 19]. This discovery has led to the proliferation of pulse oximeters based on photoplethysmography.

1.4 How Pulse Oximeters Work

The goal of pulse oximetry is to measure the fraction of hemoglobin molecules that are bound to oxygen in the pulsatile blood that is perfusing a given region of the body [20]. This quantity is known as the functional hemoglobin saturation (SaO_2) and is defined as

$$SaO_2 = \frac{HbO_2}{Hb + HbO_2} \times 100\%, \tag{1.2}$$

where Hb is the number of deoxyhemoglobin molecules in a given volume of blood and HbO_2 is the number of oxyhemoglobin molecules in the same volume of blood. The "S" in SaO_2 stands for saturation, the "a" stands for arterial, and the "O_2" stands for diatomic oxygen. While this quantity is what the pulse oximeter is trying to measure, the actual value reported by the device is sometimes referred to as SpO_2, where the "p" stands for pulse oximeter. In this work we will only use the notation SaO_2 and SvO_2, to refer to oxygen saturation in the arteries and the veins, respectively.

Modern pulse oximeters function by exploiting the time varying spectral properties of tissue that is engorged with blood in synchrony with the cardiac cycle. The challenge in pulse oximetry based on photoplethysmography is to measure oxygen saturation in the desired vascular compartment (*e.g.*, the arteries), without allowing

the signal to be effected by the optical properties of other tissues (*e.g.*, skin, bone, connective tissue, etc.) that also impinge on the path from the light source to the light detector.

The genius of the developers of pulse oximetry was to take two elementary physiological principles, and leverage them to make a device that is simple, safe, and efficacious.

1.4.1 Principle #1: Pulsatility

Principle #1 is the pulsatility of blood in the compartment of interest. For illustrative purposes, we will consider the case of measuring the oxygen saturation in the arterial compartment. We begin by identifying a time period over which the volume of blood in the compartment of interest changes while the optical absorbance due to the other tissues remains constant. In the case of the arterial system, this will be the period of the cardiac cycle. By subtracting the absorbance at its zenith from the corresponding value at its nadir, we calculate the absorbance due to the added volume of blood cycling in and out of the arteries in the region of tissue sampled by the PPG. This single principle already provides a powerful tool for isolating the physiology of the arterial system from the other tissues, affording, for example, a continuous, non-invasive measure of sympathetic tone [1].

1.4.2 Principle #2: Differential Spectral Absorbance

Principle #2 is the differential spectral absorbance of the two species we are investigating (*i.e.*, oxyhemoglobin and deoxyhemoglobin). These two molecules absorb approximately the same fraction of light in the infrared (IR); however, in the red region of the visible spectrum, deoxyhemoglobin is a much stronger absorber than

oxyhemoglobin. By calculating the change in absorbance of IR and red light simultaneously, we may infer the spectral properties of the added volume of blood. For example, if the absorbance at the red and IR wavelengths changes by a similar amount, then we can surmise that the cyclically changing blood volume primarily contains oxyhemoglobin. Conversely, if the change in absorbance is much greater at the red wavelength, then we can surmise that the relevant compartment contains primarily deoxyhemoglobin. To summarize, the change in absorbance at two wavelengths during a cyclic volume modulation in the compartment of interest enables us to calculate the fraction of hemoglobin molecules that are bound to oxygen, and hence the oxygen saturation for the blood that is in motion.

1.4.3 Calculating Oxygen Saturation Using the Photoplethysmograph Waveform

In the preceding section, we provided a qualitative description of how PPG-based pulse oximeters work. In this section, we derive a formula that relates oxygen saturation to measurable quantities, based on the analysis in Ref. [21].

When analyzing the passage of light through a sample of hemolyzed blood of thickness d and absorption constant α, we may use the Beer-Lambert law to relate the incident intensity (I_i) to the transmitted intensity (I_t) as

$$\mathrm{I}_t = \mathrm{I}_i e^{-\alpha d}. \tag{1.3}$$

In the case of a heterogeneous medium such as a biological sample, the contributions of the various tissues to the total absorption combine additively:

$$\mathrm{I}_t = \mathrm{I}_i e^{-B-\epsilon\alpha l}, \tag{1.4}$$

where B is a background term characterizing all of the tissue besides blood, and α is

the extinction coefficient in blood and l is the effective path length. In transmission mode PPG, optical scattering will make the effective path length greater than the geometric distance along a straight line connecting the optical source and detector. In reflection mode PPG, scattering is the phenomenon that determines the shape of the curved light beam connecting the source and the detector.

During one cardiac cycle, the amount of blood in the path of the light beam will fluctuate. Let $\mathrm{I_{max}}$ correspond to the maximum transmitted light intensity recorded during a cardiac cycle. Similarly, let $\mathrm{I_{min}}$ correspond to the minimum over the cardiac cycle. The intensity of detected light varies inversely with local engorgement with blood. Therefore, $\mathrm{I_{max}}$ occurs during diastole, while $\mathrm{I_{min}}$ occurs during systole. If we express the concentration at the peak of engorgement as $c_{\mathrm{max}} = c_{\mathrm{min}} + \Delta c$, we obtain a relationship between $\mathrm{I_{max}}$ and $\mathrm{I_{min}}$ that does not depend on the background absorption:

$$\mathrm{I_{min}} = \mathrm{I_{max}} e^{-\epsilon\, \Delta c\, l}, \tag{1.5}$$

which may be reexpressed as follows:

$$\ln\left(\frac{\mathrm{I_{max}}}{\mathrm{I_{min}}}\right) = \epsilon\, \Delta c\, l. \tag{1.6}$$

Let us assume that we have simultaneous measurements at two wavelengths (λ_1 and λ_2), such that $(\mathrm{I_{max}}/\mathrm{I_{min}})_1$ characterizes the absorption at λ_1, and $(\mathrm{I_{max}}/\mathrm{I_{min}})_2$ characterizes the absorption at λ_2. We now have two simultaneous equations

$$\ln\left(\frac{\mathrm{I_{max}}}{\mathrm{I_{min}}}\right)_1 = \epsilon_1\, \Delta c_1\, l_1 \tag{1.7}$$

$$\ln\left(\frac{\mathrm{I_{max}}}{\mathrm{I_{min}}}\right)_2 = \epsilon_2\, \Delta c_2\, l_2, \tag{1.8}$$

where the subscripts for ϵ, Δc, and l, identify the associated wavelength.

Given that the difference $\Delta \mathrm{I} = \mathrm{I_{max}} - \mathrm{I_{min}}$ is typically less than 3% of $\mathrm{I_{min}}$, we

may make the following approximation:

$$\ln\left(\frac{\mathrm{I_{max}}}{\mathrm{I_{min}}}\right) = \ln\left(\frac{\mathrm{I_{min}} + \Delta\mathrm{I}}{\mathrm{I_{min}}}\right) \approx \frac{\Delta\mathrm{I}}{\mathrm{I_{min}}}, \tag{1.9}$$

where we have used the Taylor expansion $\ln(1+x) = x + \mathrm{O}(x^2)$.

The quantity R is known as the "ratio of ratios," and is defined as

$$\mathrm{R} = \frac{\left(\frac{\Delta\mathrm{I}}{\mathrm{I_{min}}}\right)_1}{\left(\frac{\Delta\mathrm{I}}{\mathrm{I_{min}}}\right)_2}. \tag{1.10}$$

Equations (1.7), (1.8), and (1.9) combine to yield

$$\mathrm{R} = \frac{\epsilon_1 \, \Delta c_1 \, l_1}{\epsilon_2 \, \Delta c_2 \, l_2}. \tag{1.11}$$

If λ_1 and λ_2 are chosen such that the effective path lengths are approximately equal ($l_1 \approx l_2$) and the concentration changes are approximately equal ($\Delta c_1 \approx \Delta c_2$), then we have:

$$\mathrm{R} = \frac{\epsilon_1}{\epsilon_2}. \tag{1.12}$$

Writing the respective absorption coefficients as weighted sums of terms due to oxyhemoglobin (ϵ_o) and deoxyhemoglobin (ϵ_d), we have

$$\epsilon_x = \epsilon_{ox} \, \mathrm{SO_2} + \epsilon_{dx} \, (1 - \mathrm{SO_2}), \tag{1.13}$$

where $x = 1, 2$ identifies the relevant wavelength (λ_1 or λ_2), and $\mathrm{SO_2}$ is the oxygen saturation. Combining Eqs. (1.12) and (1.13), and solving for $\mathrm{SO_2}$, we have

$$\mathrm{SO_2} = \frac{\epsilon_{d1} - \mathrm{R}\epsilon_{d2}}{\mathrm{R}(\epsilon_{o2} - \epsilon_{d2}) - (\epsilon_{o1} - \epsilon_{d1})}. \tag{1.14}$$

Equation (1.14) achieves our goal of expressing $\mathrm{SO_2}$ in terms of the measurable quantity R (defined in Eq. (1.10)), and extinction coefficients ϵ_{yx}, where $y = o, d$ specifies oxyhemoglobin or deoxyhemoglobin, and $x = 1, 2$ specifies wavelength λ_1 or λ_2.

A crucial assumption in the preceding analysis is that the optical pathlengths traveled by the two wavelengths is approximately equal. Since the shape of the optical beams connecting the source and detectors is governed by the optical scattering at the relevant wavelength, an assumption about pathlength translates into an assumption about scattering. Unfortunately, the scattering constants associated with the most common choice of wavelengths (red and infrared) are not sufficiently close to warrant this approximation. Thus, instead of relying on relations such as that in Eq. (1.14), most pulse oximeters use an experimentally determined calibration curve established by measurements on a large group of healthy volunteers [22]. A commonly used linear approximation to these calibration curves is given by

$$SO_2 = 110 - 25\,R. \tag{1.15}$$

As the current work is an initial investigation of several novel methods for measuring oxygen saturations, we will use Eq. 1.15 exclusively in calculating SO_2 from R. One consequence of foregoing calibration is that our calculated SO_2 values will occasionally exceed 100%. In addition, signal artifact can lead to nonphysiologic saturations. Thus, we set limits for the overall saturations, such that any value under 50% is reported as 50%, and any value over 110% is reported as 110%.

1.5 Other Approaches to Measuring Venous Oxygen Saturation

The goal of this thesis is to investigate methods for using the PPG waveform to measure venous oxygen saturation. In Section 1.4, we outlined the necessary conditions for using spectroscopic measurements to infer the oxygen saturation in a given vascular compartment: (1) pulsatile flow, and (2) differential spectral absorbance. The

differential spectral absorbance of oxyhemoglobin and deoxyhemoglobin does not depend on the vascular compartment being studied. Thus, as we turn our attention to the venous compartment, condition (2) is trivially satisfied. However, regarding the pulsatility condition, there is an apparent impediment towards our goal of measuring venous oxygen saturation. Specifically, the peripheral venous compartments are conventionally thought of as lacking pulsatility. As the arteries progress to arterioles and capillaries, total cross section of the vasculature increases, resulting in a decreased resistance. Concomitant with this decrease in resistance is a transition from pulsatile flow to constant flow. Furthermore, the venous pathways connecting peripheral veins with the heart are typically interrupted by valves, which attenuate the retrograde pressure waves originating in the right heart. Later in this thesis, we shall demonstrate that, despite these considerations, it is possible to harness physiologic sources of periodic volume changes in the venous compartment. In the following section, we summarize efforts to measure venous oxygen saturation by exploiting mechanically-induced variations in volume of the venous compartment.

1.5.1 Venous Occlusion

One way to increase the volume in the venous compartment in a given appendage is to occlude the venous outflow using a pressure cuff. When the pressure applied is greater than the venous pressure but smaller than the diastolic arterial pressure, blood will continue to perfuse the appendage and will pool in the venous compartment. By comparing the spectral absorbance at two or more wavelengths before and after the occlusion, it is possible to infer the oxygen saturation of the blood that collects in the venous compartment. This approach has been experimentally demonstrated [21, 23]. In Ref. [23], the investigators compared the venous oxygen saturation they measured

via spectrophotometry with that obtained via co-oximetry (*i.e.*, the gold standard *en vitro* method) on blood samples drawn from superficial veins. Comparing the saturations obtained by these two methods, they found a significant correlation ($n = 19$, $r = 0.7$, $p < 0.0001$). Interestingly, the systematic bias they observed was dependent on the lateral spacing between the light source and the light detector, which were positioned on the same side of the limb in a reflectance configuration. They inferred that as the distance between the source and detector increased, the light beam connecting them traveled deeper into the tissue, beyond superficial arterio-venous shunts that are involved in thermoregulation. Thus, they hypothesized that the more widely spaced source and detector sample the deeper, more desaturated blood, leading to lower venous oxygen saturations.

1.5.2 High Frequency Pulsation

There are two primary disadvantages to the method described in the previous section (*i.e.*, measuring venous oxygen saturation via venous occlusion). First, the method does not allow continuous measurement, since it relies on discrete interventions separated by enough time for the tissue to reach equilibrium. Second, it requires a substantial disturbance to the local physiology, leading to potential complications such as venous stasis, venous thrombosis, and interference with intravenous access. In Ref. [9], Echiadis *et al* address these deficiencies by employing a more sophisticated method of externally modulating the volume in the venous compartment. Specifically, they use a finger pressure cuff that is driven by a pneumatic generator such that the finger experiences low pressure modulations at a frequency that does not overlap with the cardiac signal or its harmonics. A conventional PPG probe is placed on the same finger distal to the cuff. The resulting PPG waveform can then be decomposed

into the relevant spectral components such that variation at the cardiac frequency ($\sim$ 1Hz) can be isolated from variations at the pressure cuff frequency ($\sim$ 7.5Hz). At that point, the method outlined in Section 1.4 is used to calculate oxygen saturation for the arteries (using the cardiac-frequency signal) and the veins (using the pressure cuff-frequency signal).

Reference [9] reports the performance of this system in patients undergoing cardiopulmonary bypass. The venous saturation obtained via spectrophotometry is compared with the saturation measured by the CPB machine on the blood that is traveling from the patient to the machine. Since the spectrophotometric saturation is peripheral and the saturation measured by the CPB machine is central, the authors report that is not possible to infer the central venous saturation from the spectrophotometric saturation. However, the observed trends in venous oxygen saturation during changes in temperature, VO_2, and cardiac index are similar for the two methods.

2. Statement of Purpose

In Sections 1.5.1 and 1.5.2, we described methods for measuring venous oxygen saturation in which an external pressure cuff achieves the requisite pulsation of the venous compartment. It is natural to ask whether the same information can be gathered without this artificial perturbation. Specifically, are there physiological sources of pulsation in the venous compartment that can be used to satisfy the pulsatility condition described in Section 1.4.1?

It is well known that the PPG waveform is influenced by both positive pressure ventilation [24] and the peripheral venous pulsations [25]. In the case of positive pressure ventilation, we hypothesize that the effect on the PPG waveform is mediated by volume changes in the venous compartment. To test this hypothesis, we evaluate the performance of the methods VenSat, RespDC, and RespAC, all of which are designed to measure oxygen saturation using features of the PPG waveform associated with respiration. In the case of peripheral venous pulsations, it has been found that during diastole, the natural venous pulsations cause volume changes in the venous compartment to dominate those in the arterial compartment [26]. This should lead to lower overall oxygen saturation during this period between consecutive beats. To test this hypothesis, we evaluate the performance of the methods ArtInstSat, VenInstSat, and Harmonic. ArtInstSat and VenInstSat are derived from the concept of an "instantaneous saturation," in which the overall oxygen saturation is tracked throughout

the cardiac cycle. The Harmonic method is a frequency-domain technique which targets blood moving at twice the frequency of the cardiac pulse, thus attempting to incorporate the influence of diastolic pulsations.

To summarize, the purpose of this thesis is to evaluate several new methods for extracting information regarding blood oxygen saturation from the PPG waveform. These new methods will be evaluated using data collected from 10 coronary bypass graft surgery patients, as described below. A preliminary goal is to verify that the methods proposed for measuring venous oxygen saturation yield lower saturations than the methods proposed for measuring arterial oxygen saturation. A further goal is to demonstrate that the values obtained for each method are within physiologic ranges.

3. Methods

3.1 The Data Set

The data analyzed in this thesis was collected by Panayiotis A. Kyriacou and coworkers at the City University, London, UK. They developed a special-purpose esophageal PPG probe [27] and used this probe to collect PPG waveforms on patients undergoing coronary artery bypass surgery and postoperative care in the intensive care unit [28, 29]. All patients were undergoing positive pressure ventilation. The experimental protocol received institutional approval, and each patient was consented before surgery. The purpose of these investigations was to evaluate the esophagus as an alternative site for measuring oxygen saturation. Their results show that while conventional finger pulse oximeters can fail during states of relative hypoperfusion, the esophageal PPG signal remained robust, providing a reliable indication of oxygen saturation (for a review of pulse oximetry in the esophagus, see Ref. [30]).

In this work, we analyzed the esophageal PPG waveforms for ten of the cardiac surgery patients described in Ref. [28], all of whom had coronary artery disease. While many comorbidities may have an impact on oxygen saturation (*e.g.*, valvular disease, chronic obstructive pulmonary disease, congenital heart disease, ventilation/perfusion mismatch), none of these conditions were considered exclusionary. This liberal inclusion policy is in accordance with the exploratory nature of our investigation. For

each patient, approximately 100 minutes of data were collected in blocks averaging 10 minutes. These data collections occurred in the operating room, the recovery suite, and the intensive care unit.

We chose to analyze esophageal data for several reasons. Unlike the finger, the earlobe, and the forehead, the esophagus is shielded from background light, which is a substantial source of noise for PPG probes. In addition, the esophagus retains strong pulsatile blood flow during states of relative hypoperfusion, when the weak pulsatile flow at the extremities can cause conventional pulse oximeters to fail [28, 29]. Furthermore, the methods the we are investigating for measuring venous oxygen saturation depend on influence of respiration and peripheral venous pulsations which are reflecting central cardiac pulsations. The effects of respiration and peripheral venous pulsations on the PPG waveform are presumably greater for probes placed closer to the source of these effects (the lungs and the heart, respectively). In fact, the collaboration that led to our gaining access to this data began when the sponsor of this thesis (Dr. Kirk H. Shelley) recognized that the artifacts impeding the progress of Kyriacou and coworkers in measuring arterial saturation were in fact due to the motion of venous blood [31]. It was hypothesized that these artifacts could potentially be exploited to calculate venous saturation.

3.2 Technical Details of the Experimental Apparatus

The PPG probe used by Kyriacou *et al.* consisted of a miniature circuit board containing a photodetector and two LEDs with center wavelengths 655nm (Red) and 880nm (IR) [28, 29]. This unit was placed in a sterile size-20 French gauge stomach

tube and advanced down the esophagus of an anesthetized patient. Since the LEDs and the photodetector face the same direction, this is a reflectance-mode PPG probe. The two LEDs were time multiplexed by analog switches at 75Hz. The signal from the photodetector was time demultiplexed such that each wavelength could be processed independently. The signals were then divided into a slowly changing signal (denoted "DC" to evoke quasi-static direct current electronic circuits), and a rapidly changing signal (denoted "AC" to evoke time-varying alternating current electronic circuits). The DC and AC signals were created with active filters designed to concentrate energy below 0.45Hz in the DC signal, and energy above 0.45Hz in the AC signal. These four analog waveforms were sampled by a 16-bit analog-to-digital converter at 100Hz. The digital data streams were then stored on a personal computer for post-hoc analysis. Kyriacou *et al.* also recorded an EKG trace and data from an identical PPG probe placed on the finger; however, these additional waveforms will not be analyzed in the present work.

3.3 Computational Tools

Several software packages were used to analyze the data. The time-domain methods studied in this work required automated detection of the envelope of various waveforms. The envelope consists of a curve connecting the peaks of a periodic waveform and a curve connecting the troughs of the same waveform. This was accomplished using the "Cyclic Measurements" function of LabChart 7.0.3 (AdInstruments, adinstruments.com). The original waveforms along with the envelope waveforms were then analyzed in Mathematica 7.0 (Wolfram Research, wolfram.com), which was the environment in which all of the saturation calculations took place (see Appendices A and B for the relevant Mathematica code). Finally, the resulting saturation data were

analyzed for statistical significance using SPSS Statistics 17.0 (SPSS Inc., spss.com).

3.4 Algorithms for Calculating Oxygen Saturation

The algorithms examined in this work can be divided into time domain methods and frequency domain methods. The former are defined in terms of the time varying waveforms, while the latter are defined in terms of the Fourier transform of the time varying waveforms. For each method, the PPG waveforms are used to calculate an equivalent of R, the "ratio of ratios" introduced in Section 1.4. This quantity is then converted into an oxygen saturation using Eqn. 1.15.

3.4.1 Time Domain Methods

3.4.2 ArtSat: Arterial Oxygen Saturation

The ArtSat method is the conventional time domain algorithm for measuring the arterial oxygen saturation. Referring to Fig. 3.1, the ArtSat method is diagrammed on the far left. The Mathematica code for this method is contained in Appendix A, lines 54-70. In this case, the numerator of R is the peak-to-peak amplitude of the AC waveform divided by the DC offset for the Red signals. The denomenator is the corresponding quantity defined in terms of the IR AC and IR DC signals. The modulations in the AC waveforms are dominated by the volume changes in the arteries, as evidenced by the fact that they are synchronous with the cardiac cycle.

3.4.3 VenSat: Venous Oxygen Saturation

The VenSat method is diagrammed in the middle of Fig. 3.1. The Mathematica code for this method is contained in Appendix A, lines 72-86. The numerator of R is the

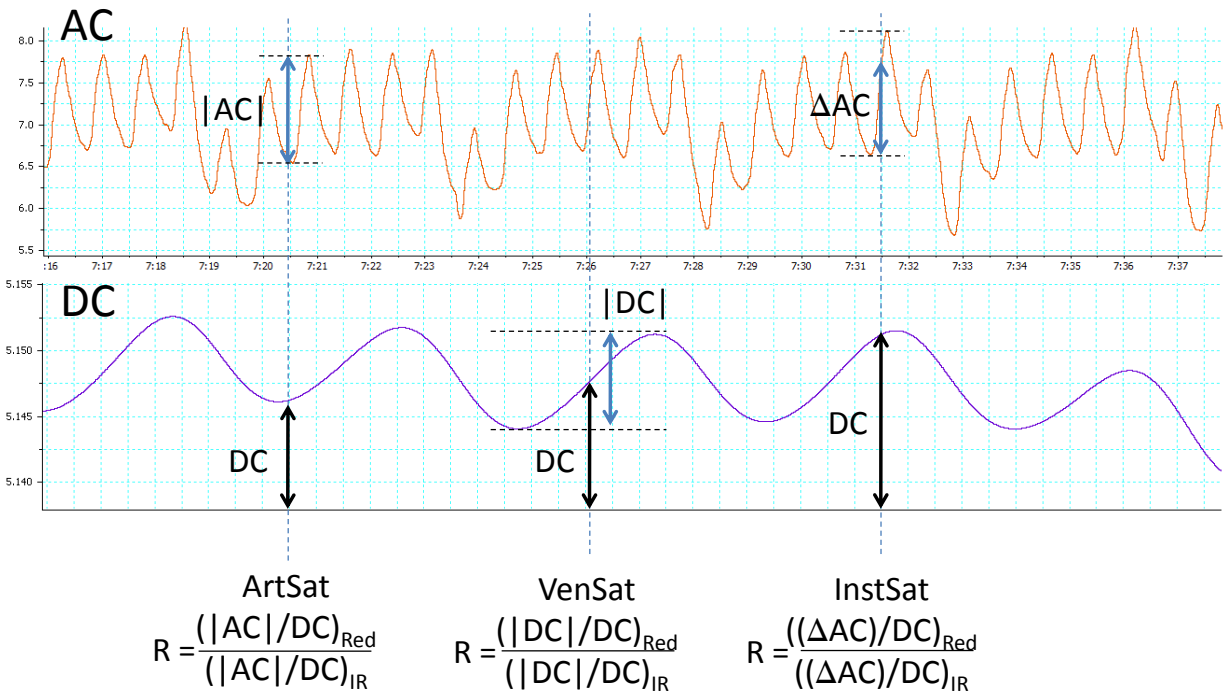

Figure 3.1 Time domain methods defined in terms of the AC and DC PPG signals. These curves represent the AC and DC signals for one wavelength (either Red or IR). For each method, the quantity R is defined in terms of the AC and DC waveforms at each wavelength. The oxygen saturation is calculated from R using Eq. 1.15. In the ArtSat method the numerator of R is the peak-to-peak amplitude of the Red AC signal divided by the value of the Red DC signal. The denomenator of R is the same quantity defined using the IR AC and IR DC signals. In the VenSat method the numerator of R is the peak-to-peak amplitude of the respiratory modulations in the Red DC signal divided by the value of the Red DC signal. As in the ArtSat method, the denomenator of R is the same quantity defined using the IR signals. In the InstSat method, the numerator of R is the height of the Red AC signal relative to the preceding trough divided by the value of the Red DC signal. As in the ArtSat and VenSat methods, the denomenator of R is the same quantity defined using the IR signals. The InstSat method yields a time varying saturation waveform which has peaks that coincide with systole and troughs that coincide with diastole. The ArtInstSat waveform is constructed by connecting the peaks these excursions. The VenInstSat waveform is constructed by connecting the troughs.

peak-to-peak amplitude of the DC waveform divided by the DC offset for the Red signals. The denomenator is the corresponding quantity defined in terms of the IR AC and IR DC signals. The modulations in the DC waveform are dominated by the influence of the positive pressure ventilation, as evidenced by the fact that they are synchronous with the 0.2Hz respirator cycle. These modulations are thought to be due to volume changes in the venous compartment. Thus, we expect the oxygen saturations calculated by this method to be lower than that calculated using the ArtSat method.

3.4.4 InstSat: Instantaneous Oxygen Saturation

The InstSat method is diagrammed on the far right of Fig. 3.1. The Mathematica code for this method is contained in Appendix A, lines 88-110. Unlike the ArtSat and VenSat methods, the InstSat method is not defined in terms of peak-to-peak amplitudes. Instead, the numerator of R is the value of the Red AC waveform minus the waveform minimum (defined as the waveform value at the preceding trough), divided by the Red DC offset. As with the previous two methods, the denomenator is the corresponding quantity defined in terms of the IR AC and IR DC signals. Unlike the ArtSat and VenSat methods, the InstSat method does not attempt to measure the oxygen saturation in one vascular compartment. Rather, it aims to provide a moment-by-moment measurement of the average saturation of the blood in all the vascular compartments in the vicinity of the probe.

One complication of the InstSat method is the inherent instability of the method near the troughs in the AC waveform. Both the numerator and the denomenator of R are proportional to the change in the AC waveform relative to the value at the preceding trough. Therefore, in the vicinity of the troughs, the numerator and

denomenator of R approach zero, and the overall fraction swings rapidly between the maximum and minimum allowable values. To address this instability, we modified the algorithm by adding a threshold feature (see the Mathematica code in Appendix A, lines 92-97). For each data point, the difference between the AC waveform and the preceding trough is compared to the DC offset. If the ratio of these two quantities is less than 0.03 (3%), the saturation calculated using these values is discarded. In that case, the saturation from the previous time is carried forward until the change in the AC waveform exceeds 3% of the DC offset. We chose 3% for the threshold because this value prevented unphysiologic swings in saturation without over-smoothing the waveform.

This thresholding procedure can be thought of as a signal-to-noise cutoff. As the change in PPG waveform approaches zero, the corresponding volume of blood in motion also approaches zero. Since the overall algorithm for calculating saturation described in Section 1.4 depends on blood in motion, the algorithm fails during the time periods when the blood is not moving. Fortunately, we may assume that the saturation of the blood in each compartment is approximately constant during these relatively short time periods. Therefore, it is permissible to carry forward the saturation from the previous time instant.

This thresholding procedure introduces artifacts in the InstSat waveform near the points at which the change in the AC waveform crosses 3% of the DC offset. Therefore, we added a smoothing procedure (see the Mathematica code in Appendix A, lines 16-20) which replaces the InstSat value with the mean of all of the InstSat values within 0.05s of the point in question.

As we will see in the Section 4, the InstSat waveform is pulsatile, with peaks approximately coinciding with the peaks in the AC waveform. In order to obtain separate information about the arterial and the venous saturation, we used LabChart

to take the envelope of the InstSat waveform, and associated the line connecting the peaks with the arterial saturation (ArtInstSat), and the line connecting the troughs with the venous saturation (VenInstSat).

3.4.5 Frequency Domain Methods

Both the time domain and frequency domain approaches to measuring oxygen saturation rely on the extraction of spectroscopic information about a region of tissue that is subject to time-varying engorgement with blood. In the time domain methods, the motion of blood is quantified by subtracting the absorption at two moments in time (*e.g.*, the peak and trough of the waveform). In the frequency domain methods, the PPG waveform is decomposed into its spectral components. For any given frequency, the relative magnitude of the spectral amplitudes for the two wavelengths (Red and IR) gives an indication of the saturation of the blood which is moving with that frequency.

The general framework for these frequency domain calculations is as follows. For each wavelength, the relevant PPG signal (either the AC or the DC) is subject to a Fourier transform. Next, the frequency of interest is identified. This choice is typically made by associating a given peak in the spectrum with a physiological source of pulsatility at that frequency (*e.g.*, the cardiac cycle, autonomic oscillations, the respiratory cycle). Once the frequency is chosen, a quantity analogous to R, the "ratio of ratios" introduced in Section 1.4, may be defined. Treating the Red signal first, the spectral amplitude at the frequency of interest is divided by the zero-frequency amplitude of the DC signal to yield the numerator of R. The corresponding quantity is calculated using the IR signal, yielding the denomenator of R. Finally, as in the time-domain cases, Eq. 1.15 is used to relate R to the corresponding oxygen

saturation.

For the frequency methods described below, the time-domain PPG waveforms are divided into one-minute segments, each of which contains 60s $\times$ 100Hz = 6000 data points. These one-minute segments are then multiplied by the Hanning window function

$$\frac{1-\cos\left(\frac{2\pi r}{6000}\right)}{2}, \tag{3.1}$$

where $r \in \{1, 6000\}$ is the time index. This windowing prevents the introduction of high frequency artifacts associated with discontinuities in the periodic extension of the one-minute segments. The Fourier transform is implemented using Mathematica's `Fourier` command, which takes a time series u_r of length n, and returns the discrete Fourier transform in the form of list v_s, also of length n, defined by

$$v_s = \frac{1}{n}\Sigma_{r=1}^{n} u_r e^{2\pi i(r-1)(s-1)/n}. \tag{3.2}$$

In order to get a real-valued R, we take the modulus of these complex numbers in our calculations.

Figure 3.2 contains an example of the Fourier transforms of a one-minute segment of the Red AC (the dashed curve) and IR AC signals (the solid curve). These curves have been normalized by dividing the raw Fourier transform by the zero-frequency term of the DC signal. Plotting the normalized spectra enables us to infer saturation information visually. The dashed curve is the numerator of R and the solid curve is the denomenator of R. Thus, if the dashed curve is higher than the solid curve (as it is at the 0.2Hz respiratory peak), then R > 1 and the saturation $SO_2 = 110 - 25R$ is less than 85%.

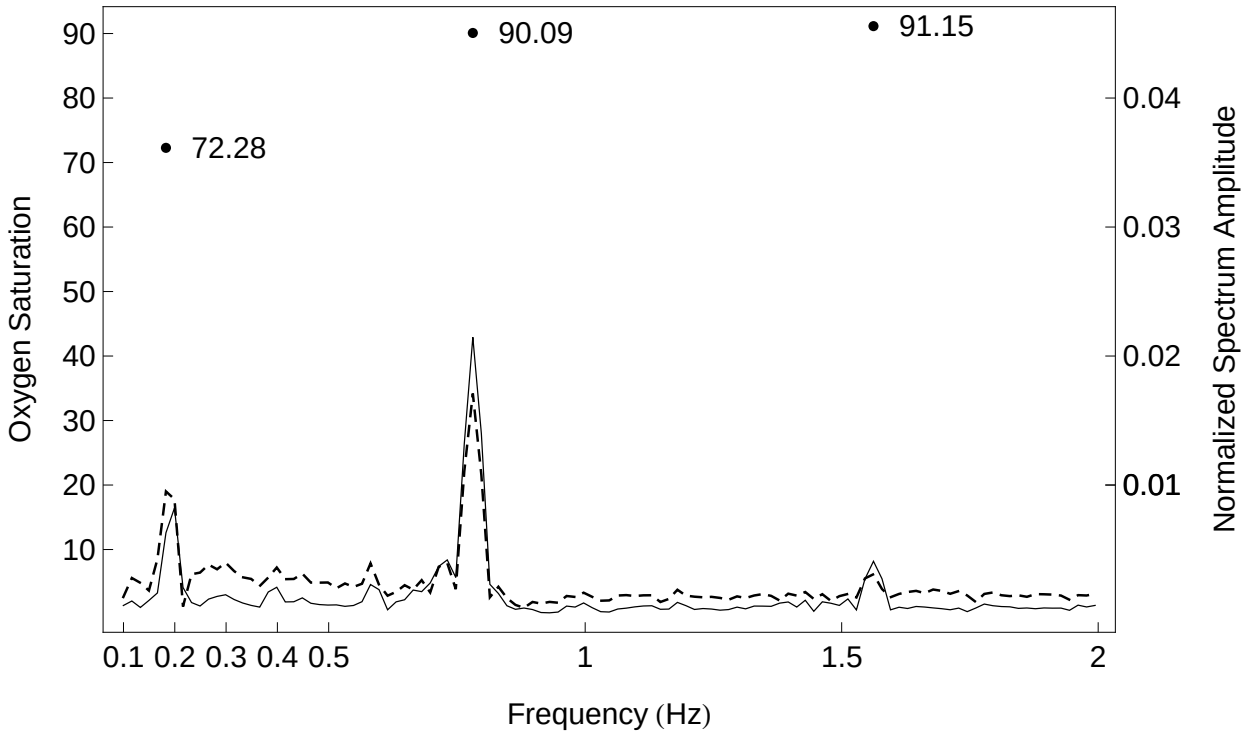

Figure 3.2 Frequency-domain methods. The dashed line is the normalized Fourier transform of one minute of the Red AC PPG signal. To normalize the signals, the entire Fourier transform is divided by the first term in the Fourier transform of the Red DC signal. The solid line is the normalized Fourier transform for the IR wavelength. As in the time-domain methods, the oxygen saturation is determined by calculating R and then using the approximation in Eq. 1.15 to relate R and oxygen saturation. In the frequency-domain methods, R is calculated by choosing a particular frequency (*e.g.*, the respiratory peak at ~ 0.2Hz), and dividing the value of the dashed curve by the value of the solid curve. Three particular frequencies are examined in this thesis: the respiratory frequency (RespDC and RespAC), the cardiac frequency (Cardiac), and the cardiac harmonic frequency (Harmonic). The saturation values for these particular frequencies are represented by the three points at the top of the figure.

3.4.6 RespDC and RespAC: Respiratory Frequency Methods

As described in Section 3.2, the experimental apparatus divides the raw PPG signal for a given wavelength into "AC" and "DC" signals. The active filters which accomplish this signal processing are designed such that the "DC" signal contains spectral components below 0.45Hz, while the "AC" signal contains spectral components above 0.45Hz. It is well known that a real-time filtering circuit cannot achieve a transfer function which completely eliminates a specified range of frequencies. For example, we see that the envelope of the AC signal in Fig. 3.1 oscillates with the same frequency as the DC signal, indicating that there is some leakage of spectral energy across the 0.45Hz threshold. Thus, in targeting the respiratory frequency, we evaluated the same algorithm on both the DC and AC signals. We denote the results of this algorithm on the DC and AC signals RespDC and RespAC, respectively. The same reasoning that led us to expect that the time-domain method VenSat would yield lower saturations suggests that RespDC and RespAC will also reflect the motion of venous blood.

The Mathematica code for the RespDC method is contained in Appendix B, lines 121-142. The algorithm first finds frequency within the range $[0.1\text{Hz}, 0.3\text{Hz}]$ at which the Fourier transform of the Red DC signal has the greatest amplitude. This peak-finding procedure is designed to identify the respiratory peak. Once this frequency is found, R is calculated as described above. Finally, the oxygen saturation is calculated using Eq. 1.15. The Mathematica code for the RespAC method is contained in Appendix B, lines 144-165. This method is identical to RespDC, except that the AC signals are used in place of the DC signals.

3.4.7 Cardiac: Oxygen Saturation at the Cardiac Frequency

The Mathematica code for the Cardiac method is contained in Appendix B, lines 167-187. The algorithm first finds frequency within the range $[0.75\text{Hz}, 2\text{Hz}]$ at which the Fourier transform of the Red AC signal has the greatest amplitude. This peak-finding procedure is designed to identify the cardiac peak. The saturation of the blood moving at this frequency is then calculated as in the previously described frequency methods. Since the cardiac frequency is associated with fluctuation in the arterial compartment, we expect the saturation obtained by this method to reflect the motion of arterial blood.

3.4.8 Harmonic: Oxygen Saturation at the Cardiac Harmonic Frequency

The Mathematica code for the Harmonic method is contained in Appendix B, lines 189-213. This algorithm is identical to the Cardiac method, except that the frequency used is twice the value of the cardiac peak, as determined by the Cardiac method. The reasoning behind looking at this frequency is as follows. The central venous pulse waveform can be transmitted through the venous system, leading to peripheral venous pulsations and the appearance of a diastolic peak in the PPG signal [25]. When such a diastolic peak is superimposed on the systolic cardiac peak, the overall signal has peaks that occur at twice the cardiac frequency. Thus, we expect the saturation of blood moving at this frequency to reflect some combination of arterial and venous saturations.

4. Results

The eight saturation algorithms described in Section 3.4 (ArtSat, VenSat, ArtInstSat, VenInstSat, RespDC, RespAC, Cardiac, and Harmonic) were applied to the esophageal PPG data recorded from ten patients undergoing cardiac surgery. Each patient record was divided into one-minute intervals. A given saturation algorithm applied to such a one-minute interval yields a time series of saturation values. The median of this set of saturation values was recorded as the value of that particular saturation algorithm applied to that particular patient over that particular minute. Thus, for each patient, a record was generated that consists of a set of eight saturation values, such that each set corresponds to one minute of recorded data. Quartile information characterizing this data is presented in Table 4.1.

The median saturations in Table 4.1 are depicted graphically in Fig. 4.1. The distribution of saturations is illustrated by the histogram at the top of the figure, and by the corresponding box-and-whisker plots at the bottom of the figure. For a given saturation algorithm, the box-and-whisker plot contains a thin vertical line which signifies the upper and lower saturation values among the ten patients. The shaded bar extends from the 25^{th} quartile to the 75^{th} quartile. The horizontal line within the shaded bar corresponds to the median saturation.

Appendix C contains histograms and box-and-whisker plots of the per-minute data gathered for each patient individually (Figs. C1-C10), as well as a cumulative

	ArtSat	VenSat	ArtInstSat	VenInstSat	RespDC	RespAC	Cardiac	Harmonic
Patient1 (97 min)	102 (99,103)	66 (59,75)	105 (104,106)	92 (79,97)	65 (59,73)	102 (99,103)	104 (97,106)	103 (97,104)
Patient2 (72 min)	104 (103,104)	68 (60,75)	106 (105,106)	99 (78,102)	70 (62,73)	102 (102,103)	105 (103,106)	105 (101,106)
Patient3 (55 min)	102 (101,104)	68 (59,73)	105 (104,107)	96 (92,98)	63 (50,67)	102 (101,103)	104 (103,105)	103 (102,104)
Patient4 (48 min)	90 (82,94)	92 (75,98)	98 (94,101)	72 (56,81)	87 (58,95)	91 (79,96)	90 (80,96)	87 (77,93)
Patient5 (67 min)	95 (90,100)	90 (72,93)	100 (95,105)	86 (73,90)	91 (78,94)	92 (88,94)	96 (89,102)	95 (85,100)
Patient6 (54 min)	100 (95,102)	75 (67,95)	103 (98,105)	91 (86,98)	76 (68,94)	99 (94,102)	101 (92,105)	98 (92,105)
Patient7 (35 min)	99 (88,103)	81 (64,93)	104 (98,106)	71 (54,93)	72 (57,89)	94 (82,102)	104 (95,106)	97 (77,106)
Patient8 (87 min)	100 (95,101)	77 (64,84)	104 (103,105)	89 (79,97)	75 (56,85)	97 (93,102)	100 (95,104)	100 (95,104)
Patient9 (48 min)	100 (95,101)	79 (74,90)	103 (102,105)	87 (81,94)	78 (72,92)	99 (89,102)	99 (89,102)	101 (92,102)
Patient10 (109 min)	101 (92,104)	81 (51,94)	105 (101,105)	81 (66,90)	76 (50,91)	100 (90,104)	100 (90,104)	101 (90,104)

Table 4.1 Quartile information characterizing the eight saturation algorithms (ArtSat, VenSat, ArtInstSat, VenInstSat, RespDC, RespAC, Cardiac, and Harmonic) applied to the esophageal PPG records of ten patients undergoing cardiac surgery. The number of minutes of data analyzed for each patient is listed under the patient identifier in the left-most column. The values in each cell correspond to the median and the 25^{th} and 75^{th} quartiles.

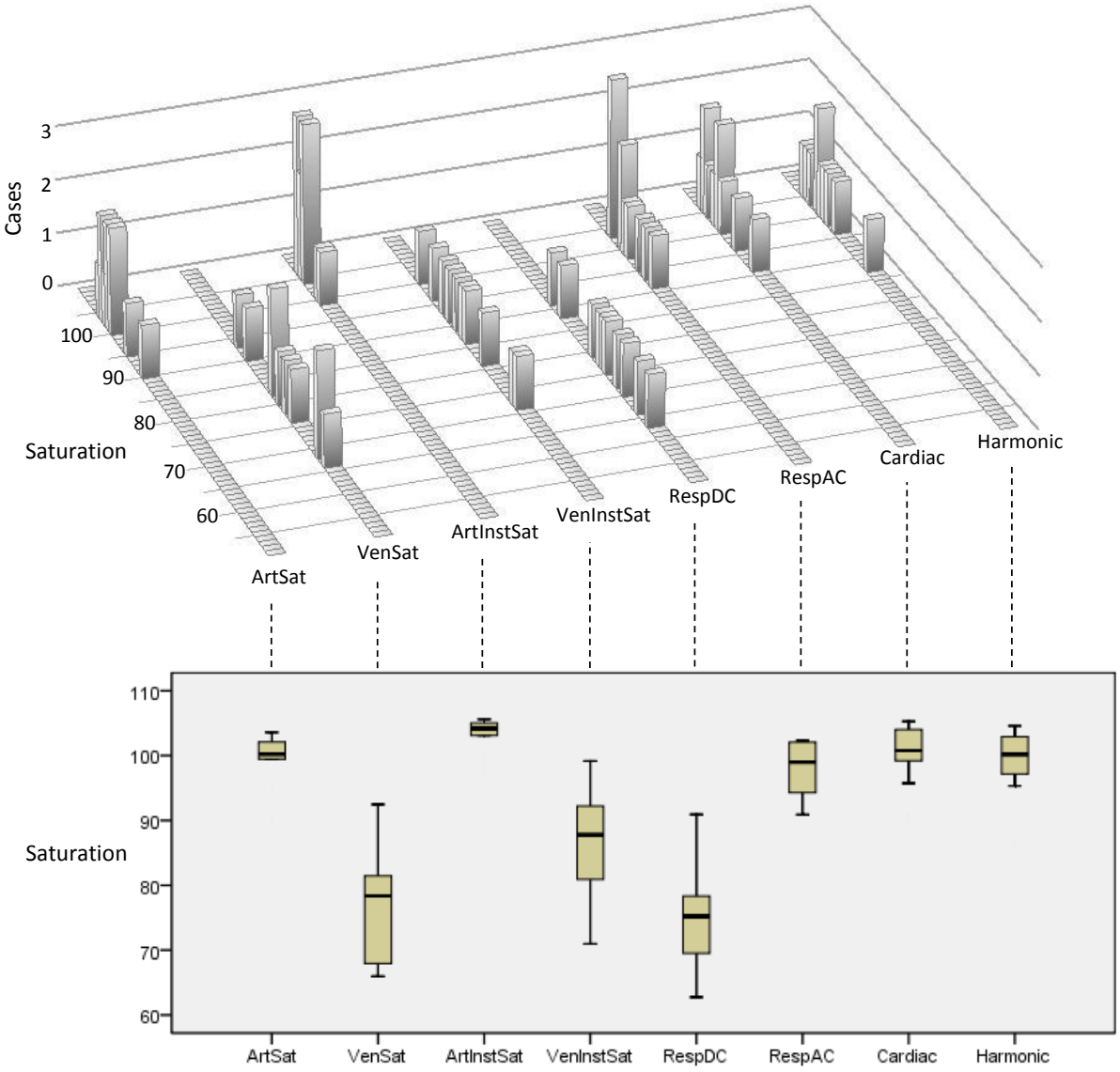

Figure 4.1 Histogram and box-and-whisker plot summarizing the median saturations reported in Table 4.1. The distribution of values for a given saturation algorithm is illustrated by the histogram at the top of the figure, and by the corresponding box-and-whisker plots at the bottom of the figure. For a given saturation algorithm, the box-and-whisker plot contains a thin vertical line which signifies the upper and lower saturation values among the ten patients. The shaded bar extends from the 25^{th} quartile to the 75^{th} quartile. The horizontal line within the shaded bar corresponds to the median saturation.

histogram and box-and-whisker plot of the per-minute data for all the patients combined (Fig. C11).

4.1 Statistical analysis

The primary goal of this thesis is to determine whether the proposed algorithms for measuring oxygen saturation yield different saturations than the conventional algorithm used for calculating arterial saturation (ArtSat). The data presented in Table 4.1 and Fig. 4.1 suggest that at least three of the proposed venous saturation algorithms (VenSat, VenInstSat, and RespDC) do indeed yield lower saturations. To show that these results are statistically significant, we compared the ArtSat method with the seven other methods (VenSat, ArtInstSat, VenInstSat, RespDC, RespAC, Cardiac, and Harmonic), using seven separate applications of the Wilcoxon signed-rank test. Because we are making multiple comparisons, we use the Bonferroni correction to define the threshold for significance as $p = 0.05/n$, where n is the number of comparisons. In our case, $n = 7$, and the threshold for significance is $p = 0.0071$. As shown in Table 4.2, four of the methods (VenSat, ArtInstSat, VenInstSat, and RespDC) show statistically significant differences from ArtSat. We examine the implications of these results in the following section.

	VenSat	ArtInstSat	VenInstSat	RespDC	RespAC	Cardiac	Harmonic
ArtSat	p=0.007*	p=0.005*	p=0.005*	p=0.005*	p=0.017	p=0.038	p=0.646

Figure 4.2 Wilcoxon signed-rank tests comparing the conventional method for measuring arterial saturation (ArtSat) with the seven other methods under investigation (VenSat, ArtInstSat, VenInstSat, RespDC, RespAC, Cardiac, and Harmonic). Using a Bonferroni correction for seven tests, the threshold for significance is $p = 0.05/7 = 0.0071$. With this definition of significance, four of the methods (VenSat, ArtInstSat, VenInstSat, RespDC, RespAC) are statistically different from ArtSat, while three (RespAC, Cardiac, Harmonic) are not.

5. Discussion

The purpose of this thesis is to evaluate several techniques for measuring venous oxygen saturation using the PPG signal. The general framework for these methods is based on the same principle that underlies conventional pulse oximetry. We first identify a vascular compartment that undergoes periodic volume changes. We then measure the change in optical absorbance that this motion produces at each of two wavelengths. This information is then combined with the known spectral properties of oxyhemoglobin and deoxyhemoglobin to infer the oxygen saturation of the blood in motion.

In conventional pulse oximetry, the detected volume change is due to the cardiac cycle. The dominant volumetric effect of the cardiac cycle on a given region of tissue is the periodic engorgement of the arterial compartment. Thus, this method is designed to measure the oxygen saturation of arterial blood. This approach can be implemented in the time domain by calculating the change in absorbance between systole and diastole (ArtSat), or in the frequency domain by comparing the strength of the cardiac peaks in the Fourier transforms of the PPG waveform at each wavelength (Cardiac).

In order to measure the oxygen saturation of venous blood, the methods that we investigate rely on two sources of volume change in the venous compartment: respiration and venous pulsations. In the case of respiration, we evaluate one time-domain method (VenSat) and two frequency-domain methods (RespDC and RespAC). In the

case of venous pulsations, we evaluate time-domain methods ArtInstSat and VenInstSat, which are derived from an "instantaneous saturation." Unlike the other methods for calculating oxygen saturation, the instantaneous saturation method yields a saturation waveform that reflects changes within a single cardiac cycle. We evaluate a frequency-domain method (Harmonic) for detecting venous pulsations by comparing the energy in the PPG at twice the cardiac frequency for each wavelength.

The first step in evaluating a given method for measuring oxygen saturation is to determine if the differences between the new method and the conventional method are statistically significant. As reported in Fig. 4.2, four of the methods (VenSat, ArtInstSat, VenInstSat, and RespDC) show statistically different saturation values when compared to the conventional method (ArtSat). Contrariwise, the remaining three methods (RespAC, Cardiac, and Harmonic) do not show statistically significant difference from ArtSat. We next discuss the results for each method individually.

As seen in Fig. 4.1, the VenSat method yields saturations that are clustered around 80%, which is within the physiologic range of venous saturations. The VenSat distribution is clearly distinct from the ArtSat distribution, which is tightly clustered around 100%. Thus, the VenSat method satisfies both of the criteria we specified for a successful demonstration. First, the saturation values are statistically distinguishable from the conventional method. Second, the saturation values are within a physiologic range for venous saturations.

RespDC and RespAC are the frequency methods that correspond to the time-domain method VenSat. RespDC involves comparing the respiratory peaks (~ 0.2Hz) of the Fourier transforms of the "DC" signals, which are produced by a filter that passes frequencies less than ~ 0.45Hz. RespAC is the same method applied to the "AC" signals, which are produced by a filter that passes frequencies greater than ~ 0.45Hz. Since RespDC is the frequency-domain equivalent of VenSat, we expect

similar saturations, and Fig. 4.1 confirms this. On the other hand, the majority of the respiratory modulation has been filtered out of the "AC" signals. One might therefore expect that the RespAC method would yield saturations close to the isobestic point (85%). This is the saturation obtained from Eq. 1.15 when the signals at the two wavelengths are identically modulated, as in the case of noise. If fact, Fig. 4.1 shows that the saturations generated by RespAC are consistent with the arterial saturations generated by ArtSat. This suggests that the filter that creates the "AC" signals does not completely extinguish frequencies below ~ 0.45Hz. Furthermore, it suggests that the pressure changes associated with respiration lead to volume changes in the arterial compartment as well as the venous compartment.

VenInstSat and ArtInstSat both yield saturations that differ from ArtSat such that the differences are statistically significant. Since the VenInstSat method is designed to track the minimum excursions of the instantaneous saturation of the blood, we would expect these saturations to be in the venous range. Indeed, we see in Fig. 4.1 that VenInstSat yields saturations that are clustered in the mid to upper 80s. The ArtInstSat method is designed to track the maximum excursions of the instantaneous saturation. It is interesting to note that this method yields saturations that are higher than those of the ArtSat method. This may be due to the fact that the conventional ArtSat method mixes some venous influence in the algorithm (venous blood is surely in motion to some degree during systole). In contrast, the ArtInstSat method may provide a closer approximation to true arterial saturation because it is sensitive to the initial influx of arterial blood at the beginning of systole.

The Cardiac method is the frequency domain equivalent of ArtSat method. Thus, is it not surprising that the difference between these two methods is not statistically significant. The Harmonic method is a frequency method that is designed to detect venous pulsations by comparing the energy in the PPG at twice the cardiac

frequency for each wavelength. As seen in Fig. 4.1, this method yields saturations that are consistent with Cardiac and ArtSat, indicating that Harmonic fails to detect venous blood. We may understand this failure in the following way. In analyzing the Fourier transforms of the PPG signals at twice the cardiac frequency we are combining the effects of the systolic pulsation with whatever diastolic pulsations are present. Thus, even if the diastolic pulsations do represent the motion of venous blood, the contribution from the motion of the arterial blood during systole will dominate the overall saturation.

The approach we have followed in this work is subject to several limitations. First, as mentioned above, the equation we use for calculating saturation interprets random noise as blood with saturation 85%. Since this value is also in the physiologic range for the saturation of venous blood, it is possible that some of the low saturations that we measure are due to noise and not the motion of venous blood. However, we can be confident that the methods which yield saturations much lower than 85% (VenSat and RespDC) are less threatened by this effect. Second, as with all PPG analysis, our methods are subject to error due to the influence of artifacts in the raw signal. These artifacts may be due to a myriad of sources, such as optical noise, electrical noise, and motion artifacts. Third, the methods we investigate here rely on automated algorithms that are designed to detect the peaks and troughs of the PPG waveforms. When the PPG waveforms depart from sinusoidal behavior, these algorithms can provide spurious results. Fourth, the lack of a calibration step in the calculation of our saturations leads to values that range above the logical maximum (100%) and below the physiological reasonable minimum (50%).

Despite these limitations, it is still possible to make provisional conclusions in light of our results. Specifically, we have provided strong evidence that it is possible to gain information concerning the oxygen saturation of venous blood via analysis of

the esophageal PPG waveform. The clearest demonstration of this effect is seen in the methods that target the respiratory cycle (VenSat and RespDC). The low saturations measured by these methods strongly support the hypothesis that the effect of positive pressure ventilation on the PPG waveform is mediated predominately by volume changes in the venous compartment.

It is premature to assess the clinical implications of the results presented here. In order to use these venous saturation methods to infer other physiological parameters as described in Section 1.2, it will be necessary to compare these methods with a gold standard, such as blood gas analysis or co-oximetry. Nonetheless, given that we have strong evidence that we can detect the motion of venous blood, it is plausible that a calibration step similar to that used in pulse oximetry would enable our methods to provide accurate, real-time, noninvasive measurement of regional venous oxygen saturation.

An important difference between the traditional methods for measuring arterial saturation and the methods we present here for measuring venous saturation is that the arterial saturations are presumed to be the same throughout the body, while the venous saturations depend on numerous local features of the tissue being studied. Instead of obtaining a surrogate for mixed venous saturation, these methods yield information about the venous blood in the particular region of the body that is illuminated by the PPG probe. The mixed venous saturation is known to provide valuable clinical information, for example in contributing to the early goal-directed therapy algorithm. Thus, it may seem that regional venous saturation is less useful in a clinical setting. However, there are two factors that mitigate this criticism. First, by combining the regional venous saturation information from several PPG probes (finger, esophagus, earlobe, forehead), it may be possible to generate a surrogate for true mixed venous saturation. Second, there may be clinical settings in which regional

venous saturation is preferable to mixed venous saturation. For example, given the predominate sympathetic innervation of the extremities, early signs of shock may be evident in the venous saturation of blood in the finger before other parts of the body are affected. In addition, regional venous saturation might facilitate better monitoring of the health of a surgical skin flap as reflected by its oxygen utilization.

Looking to the future, an important step in refining these methods is to obtain the raw PPG signal, before it is decomposed into the "DC" and "AC" waveforms. This will remove the ambiguity that arises due the relative proximity of important spectral features (*i.e.*, the respiratory peak at 0.2Hz) and the filter cutoff frequency 0.45Hz. In addition, it will be necessary to evaluate these methods using PPG data collected from sites other than the esophagus. Furthermore, as mentioned above, it will be crucial to compare these methods for measuring venous saturation against a gold standard. This will also entail designing experimental methods for altering the venous oxygen saturation in the vicinity of the PPG probe. Such methods might include changing the inspired oxygen fraction or changing the elevation and/or temperature of the relevant limb.

References

[1] Shelley KH, Shelley S. Pulse oximeter waveform: Photoelectric plethysmography. In: Clinical Monitoring: Practical Applications for Anesthesia and Critical Care, Lake CL, Hines RL, Blitt CD, eds. Philadelphia PA: W.B. Saunders Company, 2001 420–428.

[2] Allen J. Photoplethysmography and its application in clinical physiological measurement. Physiol Meas 2007;28:R1–39.

[3] Murray WB, Foster PA. The peripheral pulse wave - information overlooked. J Clin Monit Comput 1996;12:365–377.

[4] Shelley KH. Photoplethysmography: beyond the calculation of arterial oxygen saturation and heart rate. Anesth Analg 2007;105:S31–6.

[5] Reinhart K, Bloos F. The value of pulse oximetry. Curr Opin Crit Care 2005; 11:259–263.

[6] Kawakami Y, Kishi F, Yamamoto H, Miyamoto K. Relation of oxygen delivery, mixed venous oxygenation, and pulmonary hemodynamics to prognosis in chronic obstructive pulmonary disease. N Engl J Med 1983;308:1045–9.

[7] Quaresimaa V, Colierc WNJM, Sluijsb Mvd, Ferraria M. Nonuniform quadriceps O2 consumption revealed by near infrared multipoint measurements. Biochem Biophys Res Commun 2001;285:1034–1039.

[8] Sise MJ, Hollingsworth P, Brimm JE, Peters RM, Virgilio RW, Shackford SR. Complications of the flow-directed pulmonary-artery catheter: A prospective analysis in 219 patients. Crit Care Med 1981;9:315–318.

[9] Echiadis AS, Crabtree VP, Bence J, et al. Non-invasive measurement of peripheral venous oxygen saturation using a new venous oximetry method: evaluation during bypass in heart surgery. Physiol Meas 2007;28:897–911.

[10] Challoner A. Photoelectric plethysmography for estimating cutaneous blood flow. In: Non-Invasive Physiological Measurements, Rolfe P, ed., vol. 1. London: Academic, 1979 125–51.

[11] Hertzman AB. Photoelectric plethysmography of the nasal septum in man. Proc Soc Exp Biol Med 1937;37:290–292.

[12] Hertzman AB. Photoelectric plethysmography of the fingers and toes in man. Proc Soc Exp Biol Med 1937;37:529–542.

[13] Hertzman AB. The blood supply of various skin areas as estimated by the photoelectric plethysmograph. Am J Physiol 1938;124:328–340.

[14] Foster AJ, Neuman C, Rovenstine E. Peripheral circulation during anesthesia, shock and hemorrage; the digital plethysmograph as a clinical guide. Anesthesiology 1945;6:246–257.

[15] Johnstone M. The effects of sedation on the digital plethysmogram. Anaesthesia 1967;22:3–15.

[16] Dahn I, Jonson B, Nilsen R. Plethysmographic in vivo determinations of elastic properties of arteries in man. J Appl Physiol 1970;28:328–32.

[17] Challoner A, Ramsay C. A photoelectric plethysmograph for the measurement of cutaneous blood flow. Phys Med Biol 1974;19:317–328.

[18] Aoyagi T, Kiahi M, Yamaguchi K, Watanabe S. Improvements of the earpiece oximeter. In: Abstracts of the 13th Annual Meeting of the Japanese Society of Medical Electronics and Biological Engineering, vol. 90. 1974 1.

[19] Yoshiya I, Shimada Y, Tanaka K. Spectrophotometric monitoring of arterial oxygen saturation in the fingertip. Med Biol Eng Comput 1980;18:27–32.

[20] Moyle JTB. Pulse Oximetry. 2nd ed. London: BMJ Books, 2002.

[21] Nitzan M, Babchenko A, Khanokh B, Taitlebaum H. Measurement of oxygen saturation in venous blood by dynamic near infrared spectroscopy. J Biomed Opt 2000;5:155–162.

[22] Webster JG. Design of Pulse Oximeters. Bristol: Institute of Physics Publishing, 1997.

[23] Yoxall CW, Weindling AM. Measurement of venous oxyhaemoglobin saturation in the adult human forearm by near infrared spectroscopy with venous occlusion. Med Biol Eng Comput 1997;35:331–336.

[24] Natalini G, Rosano A, Franceschetti ME, Facchetti P, Bernardini A. Variations in arterial blood pressure and photoplethysmography during mechanical ventilation. Anesth Analg 2006;103:1182–1188.

[25] Shelley KH, Dickstein M, Shulman SM. The detection of peripheral venous pulsation using the pulse oximeter as a plethysmograph. J Clin Monit 1993; 9:283–7.

[26] Shelley KH, Tamai D, Jablonka D, Gesquiere M, Stout RG, Silverman DG. The effect of venous pulsation on the forehead pulse oximeter wave form as a possible source of error in spo2 calculation. Anesth Analg 2005;100:743–747.

[27] Kyriacou PA, Moye AR, Gregg A, Choi DM, Langford RM, Jones DP. A system for investigating oesophageal photoplethysmographic signals in anaesthetised patients. Med Biol Eng Comput 1999;37:639–43.

[28] Kyriacou PA, Powell S, Langford RM, Jones DP. Investigation of oesophageal photoplethysmographic signals and blood oxygen saturation measurements in cardiothoracic surgery patients. Physiol Meas 2002;23:533–45.

[29] Kyriacou PA, Powell SL, Jones DP, Langford RM. Evaluation of oesophageal pulse oximetry in patients undergoing cardiothoracic surgery. Anaesthesia 2003; 58:422–7.

[30] Kyriacou PA. Pulse oximetry in the oesophagus. Physiol Meas 2006;27:R1–R35.

[31] Phillips JP, Kyriacou PA, Jones DP, Shelley KH, Langford RM. Pulse oximetry and photoplethysmographic waveform analysis of the esophagus and bowel. Curr Opin Anaesthesiol 2008;21:779–783.

Appendix A: Mathematica Code for Time Domain Methods

```
(*threshold for signal to noise filtering for instsat *)
threshold = 0.03;

(* Some general pulse ox calculation functions *)
satFromR[r_] := 110 - 25*r;
(* satFromR[r_]:=100*(1000-550*r)/(900-350*r); *)
lowerSat = 50;
higherSat = 110;
boundedSat[s_] :=
  If[s > higherSat, higherSat, If[s < lowerSat, lowerSat, s]];
 (*boundedSat[s_]:=s;**)
defaultSat = 90; (*this value used when there is a zero in the \
denomenator of the sat formula *)

(*some general functions*)
smoothList[list_, halfWindow_] := Join[
  Take[list, halfWindow],
  Table[Mean[list[[i - halfWindow ;; i + halfWindow]]], {i,
    halfWindow + 1, Length[list] - halfWindow}],
  Take[list, -halfWindow]]
constructMeans[list_, windowSize_] :=
  Table[N[Mean[list[[i ;; i + windowSize - 1]]]], {i, 1,
    windowSize*Floor[Length[list]/windowSize], windowSize}];
constructMedians[list_, windowSize_] :=
  Table[N[Median[list[[i ;; i + windowSize - 1]]]], {i, 1,
    windowSize*Floor[Length[list]/windowSize], windowSize}];

(* extracting the header and the data from the LabChart file *)
```

```
chartFileHeader =
 ReadList[chartFileName, Record, 5, RecordLists -> True]
ToExpression[
  Drop[ReadList[chartFileName, Word, RecordLists -> True], 5]];
chartFileData =
  Transpose[
   ToExpression[
    Drop[ReadList[chartFileName, Word, RecordLists -> True], 5]]];
channelLabels = Flatten[StringSplit[chartFileHeader[[4]], {"\t"}]];
numberOfDataPoints = Length[chartFileData[[1]]];

(* defining channel variables *)
oesoIRDC = chartFileData[[2]];
oesoRedDC = chartFileData[[3]];
oesoRedAC = chartFileData[[4]];
oesoIRAC = chartFileData[[5]];
oesoIRACMin = chartFileData[[6]];
oesoIRACHeight = chartFileData[[7]];
oesoRedACMin = chartFileData[[8]];
oesoRedACHeight =chartFileData[[9]];
oesoIRDCMin = chartFileData[[10]];
oesoIRDCHeight = chartFileData[[11]];
oesoRedDCMin = chartFileData[[12]];
oesoRedDCHeight = chartFileData[[13]];

(* adding a new channel -- Arterial Saturation -- AC height over DC*)


artSat = Table[
   If[oesoRedACHeight[[i]] == 0 || oesoRedDC[[i]] == 0 ||
     oesoIRACHeight[[i]] == 0 || oesoIRDC[[i]] == 0, defaultSat,
    boundedSat[
     satFromR[(oesoRedACHeight[[i]]/
         oesoRedDC[[i]])/(oesoIRACHeight[[i]]/oesoIRDC[[i]])]]
    ]
   , {i, numberOfDataPoints}];
chartFileData = Append[chartFileData, artSat];
(* updating the header to reflect the new channel *)
chartFileHeader[[4]][[1]] =
 StringJoin[{chartFileHeader[[4]][[1]], "\t|AC|/DC"}];
chartFileHeader[[5]][[1]] =
 StringJoin[{chartFileHeader[[5]][[1]], "\t10.000 V"}];
```

```
71
72  (* adding a new channel -- Venous Saturation -- DC height over DC*)
73  venSat = Table[
74     If[oesoRedDCHeight[[i]] == 0 || oesoRedDC[[i]] == 0 ||
75       oesoIRDCHeight[[i]] == 0 || oesoIRDC[[i]] == 0, defaultSat,
76      boundedSat[
77       satFromR[(oesoRedDCHeight[[i]]/
78           oesoRedDC[[i]])/(oesoIRDCHeight[[i]]/oesoIRDC[[i]])]]
79      ]
80     , {i, numberOfDataPoints}];
81  chartFileData = Append[chartFileData, venSat];
82  (* updating the header to reflect the new channel *)
83  chartFileHeader[[4]][[1]] =
84   StringJoin[{chartFileHeader[[4]][[1]], "\t|DC|/DC"}];
85  chartFileHeader[[5]][[1]] =
86   StringJoin[{chartFileHeader[[5]][[1]], "\t10.000 V"}];
87
88  (* adding a new channel -- Instantaneous Saturation -- AC change over \
89  DC with threshold*)
90  oldSat = defaultSat;
91  smoothedInstSat = smoothList[Table[
92      If[oesoRedAC[[i]] - oesoRedACMin[[i]] == 0 ||
93        oesoRedDC[[i]] == 0 || oesoIRAC[[i]] - oesoIRACMin[[i]] == 0 ||
94        oesoIRDC[[i]] == 0, oldSat,
95       If[(oesoRedAC[[i]] - oesoRedACMin[[i]])/oesoRedDC[[i]] <
96          threshold || (oesoIRAC[[i]] - oesoIRACMin[[i]])/
97           oesoIRDC[[i]] < threshold, oldSat,
98        oldSat =
99         boundedSat[
100         satFromR[((oesoRedAC[[i]] - oesoRedACMin[[i]])/
101             oesoRedDC[[i]])/((oesoIRAC[[i]] - oesoIRACMin[[i]])/
102             oesoIRDC[[i]])]]]
103      ]
104     , {i, numberOfDataPoints}], 5];
105 chartFileData = Append[chartFileData, smoothedInstSat];
106 (* updating the header to reflect the new channel *)
107 chartFileHeader[[4]][[1]] =
108  StringJoin[{chartFileHeader[[4]][[1]], "\tsmoothedInstSat"}];
109 chartFileHeader[[5]][[1]] =
110  StringJoin[{chartFileHeader[[5]][[1]], "\t10.000 V"}];
111
112 (* extracting the channel labels *)
```

```
channelLabels = Flatten[StringSplit[chartFileHeader[[4]], {"\t"}]];

masterList = Table[i, {i, Length[channelLabels] - 1}];
masterList = {1, 2, 3, 4, 13, 14, 15};

(* choosing which channels will go in output LabChart file *)
printList = masterList;
chartFileHeaderToPrint = chartFileHeader;
channelLabelsTest = Flatten[StringSplit[chartFileHeader[[4]], {"\t"}]];
channelRangeTest = Flatten[StringSplit[chartFileHeader[[5]], {"\t"}]];
chartFileHeaderToPrint[[4]][[1]] =
  StringJoin[
   Riffle[Prepend[Part[channelLabelsTest, printList + 1],
     "ChannelTitle="], "\t"]];
chartFileHeaderToPrint[[5]][[1]] =
  StringJoin[
   Riffle[Prepend[Part[channelRangeTest, printList + 1], "Range="],
    "\t"]];
chartFileDataToPrint = Part[chartFileData, Prepend[printList + 1, 1]];

(* writing the new LabChart file *)
outputStream = OpenWrite[outPutFile];
Do[{WriteString[outputStream, chartFileHeaderToPrint[[i]][[1]]],
   WriteString[outputStream, "\n"]}, {i, 5}];
WriteString[outputStream,
  ExportString[Transpose[chartFileDataToPrint], "Table"]];
Close[outputStream];
```

Appendix B: Mathematica Code for Frequency Domain Methods

```
(* specifying the input and output files *)

chartFileName = "C12 block5 output2.txt";
outPutFile = "C12 block5 batch3.txt";

SetDirectory["C:\Users\Zac\Documents\Mathematica"];

(* Some general pulse ox calculation functions *)
satFromR[r_] := 110 - 25*r;
(* satFromR[r_]:=100*(1000-550*r)/(900-350*r); *)
lowerSat = 50;
higherSat = 110;
boundedSat[s_] :=
  If[s > higherSat, higherSat, If[s < lowerSat, lowerSat, s]];
 (*boundedSat[s_]:=s;**)
defaultSat = 90; (*this value used when there is a zero in the \
denomenator of the sat formula *)

(*some general functions*)
smoothList[list_, halfWindow_] := Join[
  Take[list, halfWindow],
  Table[Mean[list[[i - halfWindow ;; i + halfWindow]]], {i,
    halfWindow + 1, Length[list] - halfWindow}],
  Take[list, -halfWindow]]
constructMeans[list_, windowSize_] :=
  Table[N[Mean[list[[i ;; i + windowSize - 1]]]], {i, 1,
    windowSize*Floor[Length[list]/windowSize], windowSize}];
constructMedians[list_, windowSize_] :=
  Table[N[Median[list[[i ;; i + windowSize - 1]]]], {i, 1,
    windowSize*Floor[Length[list]/windowSize], windowSize}];

```

```
(* extracting the header and the data from the LabChart file *)
chartFileHeader =
 ReadList[chartFileName, Record, 5, RecordLists -> True]
ToExpression[
  Drop[ReadList[chartFileName, Word, RecordLists -> True], 5]];
chartFileData =
  Transpose[
   ToExpression[
    Drop[ReadList[chartFileName, Word, RecordLists -> True], 5]]];
channelLabels = Flatten[StringSplit[chartFileHeader[[4]], {"\t"}]];
numberOfDataPoints = Length[chartFileData[[1]]];

(* defining channel variables *)
oesoIRDC = chartFileData[[2]]; oesoRedDC =
 chartFileData[[3]]; oesoRedAC = chartFileData[[4]]; oesoIRAC =
 chartFileData[[5]];
artSat = chartFileData[[6]];
venSat = chartFileData[[7]];
smoothedInstSatMax = chartFileData[[9]]; smoothedInstSatMin =
 chartFileData[[10]];

(* extracting the channel labels *)
channelLabels = Flatten[StringSplit[chartFileHeader[[4]], {"\t"}]];

masterList = {6, 7};

masterList = Table[i, {i, Length[channelLabels] - 1}];

(* specify which channels will be displayed *)
displayList = masterList;

Show[GraphicsColumn[
  Table[ListLinePlot[chartFileData[[channelIndex + 1]], Frame -> True,
     Axes -> False, AspectRatio -> 0.1,
    FrameTicks -> {{True, False}, {False, False}},
    FrameLabel -> {,
      Text[Style[
        ToString[
         ToString[channelIndex] <> " : " <>
          channelLabels[[channelIndex + 1]]], FontSize -> 10]]},
    FrameTicks -> None], {channelIndex, displayList}], Spacings -> -5,
   Alignment -> {Left, Center}]]
```

```
74
75  hanningWindow[list_] :=
76   Table[list[[i]] (1 - Cos[i*2 Pi/Length[list]])/2, {i, Length[list]}]
77  samplingFrequency = 100;
78  convertFromFrequencyToMatrixPosition[frequency_, numberOfTimeValues_,
79     localSamplingFrequency_] :=
80    Round[frequency*(numberOfTimeValues/2 - 1)/(localSamplingFrequency/
81          2) + 1];
82
83  respiratoryCardiacHarmonic[redAC_, redDC_, irAC_, irDC_,
84    localSamplingFrequency_] :=
85   {
86    localNumberOfDataPoints = Length[redAC];
87    spectrumOesoRedACW =
88     Take[Abs[Fourier[hanningWindow[redAC]]], {1,
89       Round[localNumberOfDataPoints/2]}];
90    spectrumOesoRedDCW =
91     Take[Abs[Fourier[hanningWindow[redDC]]], {1,
92       Round[localNumberOfDataPoints/2]}];
93    spectrumOesoIRACW =
94     Take[Abs[Fourier[hanningWindow[irAC]]], {1,
95       Round[localNumberOfDataPoints/2]}];
96    spectrumOesoIRDCW =
97     Take[Abs[Fourier[hanningWindow[irDC]]], {1,
98       Round[localNumberOfDataPoints/2]}];
99
100   normalizedSpectrumRedAC =
101    Table[{(i -
102         1)*(localSamplingFrequency/2)/(localNumberOfDataPoints/2 - 1),
103      spectrumOesoRedACW[[i]]/spectrumOesoRedDCW[[1]]}, {i, 1,
104      Round[localNumberOfDataPoints/2]}];
105   normalizedSpectrumRedDC =
106    Table[{(i -
107         1)*(localSamplingFrequency/2)/(localNumberOfDataPoints/2 - 1),
108      spectrumOesoRedDCW[[i]]/spectrumOesoRedDCW[[1]]}, {i, 1,
109      Round[localNumberOfDataPoints/2]}];
110   normalizedSpectrumIRAC =
111    Table[{(i -
112         1)*(localSamplingFrequency/2)/(localNumberOfDataPoints/2 - 1),
113      spectrumOesoIRACW[[i]]/spectrumOesoIRDCW[[1]]}, {i, 1,
114      Round[localNumberOfDataPoints/2]}];
115   normalizedSpectrumIRDC =
```

```
 Table[{(i -
      1)*(localSamplingFrequency/2)/(localNumberOfDataPoints/2 - 1),
    spectrumOesoIRDCW[[i]]/spectrumOesoIRDCW[[1]]}, {i, 1,
   Round[localNumberOfDataPoints/2]}];

(* get Sat at respiratory frequency from DC signals *)
minRespFrequency = .1;
maxRespFrequency = .3;
localRespMax =
 normalizedSpectrumRedDC[[
   convertFromFrequencyToMatrixPosition[minRespFrequency,
    localNumberOfDataPoints, localSamplingFrequency]]][[2]];
localRespMaxIndex =
 convertFromFrequencyToMatrixPosition[minRespFrequency,
  localNumberOfDataPoints, localSamplingFrequency];
Do[If[normalizedSpectrumRedDC[[i]][[2]] > localRespMax,
  localRespMax = normalizedSpectrumRedDC[[i]][[2]];
  localRespMaxIndex = i], {i,
  convertFromFrequencyToMatrixPosition[minRespFrequency,
   localNumberOfDataPoints, localSamplingFrequency],
  convertFromFrequencyToMatrixPosition[maxRespFrequency,
   localNumberOfDataPoints, localSamplingFrequency]}];
p0x = N[normalizedSpectrumRedDC[[localRespMaxIndex]][[1]]];
p0y = boundedSat[
  satFromR[
   normalizedSpectrumRedDC[[localRespMaxIndex]][[2]]/
    normalizedSpectrumIRDC[[localRespMaxIndex]][[2]]]];

(* get Sat at respiratory frequency from AC signals *)
minRespFrequency = .1;
maxRespFrequency = .3;
localRespMax =
 normalizedSpectrumRedAC[[
   convertFromFrequencyToMatrixPosition[minRespFrequency,
    localNumberOfDataPoints, localSamplingFrequency]]][[2]];
localRespMaxIndex =
 convertFromFrequencyToMatrixPosition[minRespFrequency,
  localNumberOfDataPoints, localSamplingFrequency];
Do[If[normalizedSpectrumRedAC[[i]][[2]] > localRespMax,
  localRespMax = normalizedSpectrumRedAC[[i]][[2]];
  localRespMaxIndex = i], {i,
  convertFromFrequencyToMatrixPosition[minRespFrequency,
```

```
158       localNumberOfDataPoints, localSamplingFrequency],
159      convertFromFrequencyToMatrixPosition[maxRespFrequency,
160       localNumberOfDataPoints, localSamplingFrequency]}];
161    p1x = N[normalizedSpectrumRedAC[[localRespMaxIndex]][[1]]];
162    p1y = boundedSat[
163      satFromR[
164       normalizedSpectrumRedAC[[localRespMaxIndex]][[2]]/
165        normalizedSpectrumIRAC[[localRespMaxIndex]][[2]]]];
166
167    minCardiacFrequency = .75;
168    maxCardiacFrequency = 2;
169    localCardiacMax =
170     normalizedSpectrumRedAC[[
171       convertFromFrequencyToMatrixPosition[minCardiacFrequency,
172        localNumberOfDataPoints, localSamplingFrequency]]][[2]];
173    localCardiacMaxIndex =
174     convertFromFrequencyToMatrixPosition[minCardiacFrequency,
175      localNumberOfDataPoints, localSamplingFrequency];
176    Do[If[normalizedSpectrumRedAC[[i]][[2]] > localCardiacMax,
177      localCardiacMax = normalizedSpectrumRedAC[[i]][[2]];
178      localCardiacMaxIndex = i], {i,
179      convertFromFrequencyToMatrixPosition[minCardiacFrequency,
180       localNumberOfDataPoints, localSamplingFrequency],
181      convertFromFrequencyToMatrixPosition[maxCardiacFrequency,
182       localNumberOfDataPoints, localSamplingFrequency]}];
183    p2x = N[normalizedSpectrumRedAC[[localCardiacMaxIndex]][[1]]];
184    p2y = boundedSat[
185      satFromR[
186       normalizedSpectrumRedAC[[localCardiacMaxIndex]][[2]]/
187        normalizedSpectrumIRAC[[localCardiacMaxIndex]][[2]]]];
188
189    minHarmonicFrequency =
190     2*N[normalizedSpectrumRedAC[[localCardiacMaxIndex]][[1]]] - 0.5;
191    maxHarmonicFrequency =
192     2*N[normalizedSpectrumRedAC[[localCardiacMaxIndex]][[1]]] + 0.5;
193    localHarmonicMax =
194     normalizedSpectrumRedAC[[
195       convertFromFrequencyToMatrixPosition[minHarmonicFrequency,
196        localNumberOfDataPoints, localSamplingFrequency]]][[2]];
197    localHarmonicMaxIndex =
198     convertFromFrequencyToMatrixPosition[minHarmonicFrequency,
199      localNumberOfDataPoints, localSamplingFrequency];
```

```
200     Do[If[normalizedSpectrumRedAC[[i]][[2]] > localHarmonicMax,
201       localHarmonicMax = normalizedSpectrumRedAC[[i]][[2]];
202       localHarmonicMaxIndex = i], {i,
203       convertFromFrequencyToMatrixPosition[minHarmonicFrequency,
204        localNumberOfDataPoints, localSamplingFrequency],
205       convertFromFrequencyToMatrixPosition[maxHarmonicFrequency,
206        localNumberOfDataPoints, localSamplingFrequency]}];
207     p3x = N[normalizedSpectrumRedAC[[localHarmonicMaxIndex]][[1]]];
208     p3y = boundedSat[
209       satFromR[
210        normalizedSpectrumRedAC[[localHarmonicMaxIndex]][[2]]/
211         normalizedSpectrumIRAC[[localHarmonicMaxIndex]][[2]]]];
212     {p0y, p1y, p2y, p3y}
213     }
214
215   batchTimeWindow = 60*samplingFrequency;
216   batchedChartFileData =
217     Table[Join[
218       Flatten[respiratoryCardiacHarmonic[
219         oesoRedAC[[i ;; i + batchTimeWindow - 1]],
220         oesoRedDC[[i ;; i + batchTimeWindow - 1]],
221         oesoIRAC[[i ;; i + batchTimeWindow - 1]],
222         oesoIRDC[[i ;; i + batchTimeWindow - 1]], samplingFrequency]], {
223        Median[artSat[[i ;; i + batchTimeWindow - 1]]],
224        Median[venSat[[i ;; i + batchTimeWindow - 1]]],
225        Median[smoothedInstSatMax[[i ;; i + batchTimeWindow - 1]]],
226        Median[smoothedInstSatMin[[i ;; i + batchTimeWindow - 1]]]
227        }], {i, 1,
228       batchTimeWindow*Floor[numberOfDataPoints/batchTimeWindow],
229       batchTimeWindow}];
230
231   (* writing the seven sats into a plain text file *)
232   outputStream = OpenWrite[outPutFile];
233   WriteString[outputStream, ExportString[batchedChartFileData, "Table"]];
234   Close[outputStream];
```

Appendix C: Histograms and Box-and-Whisker Plots for Each Patient

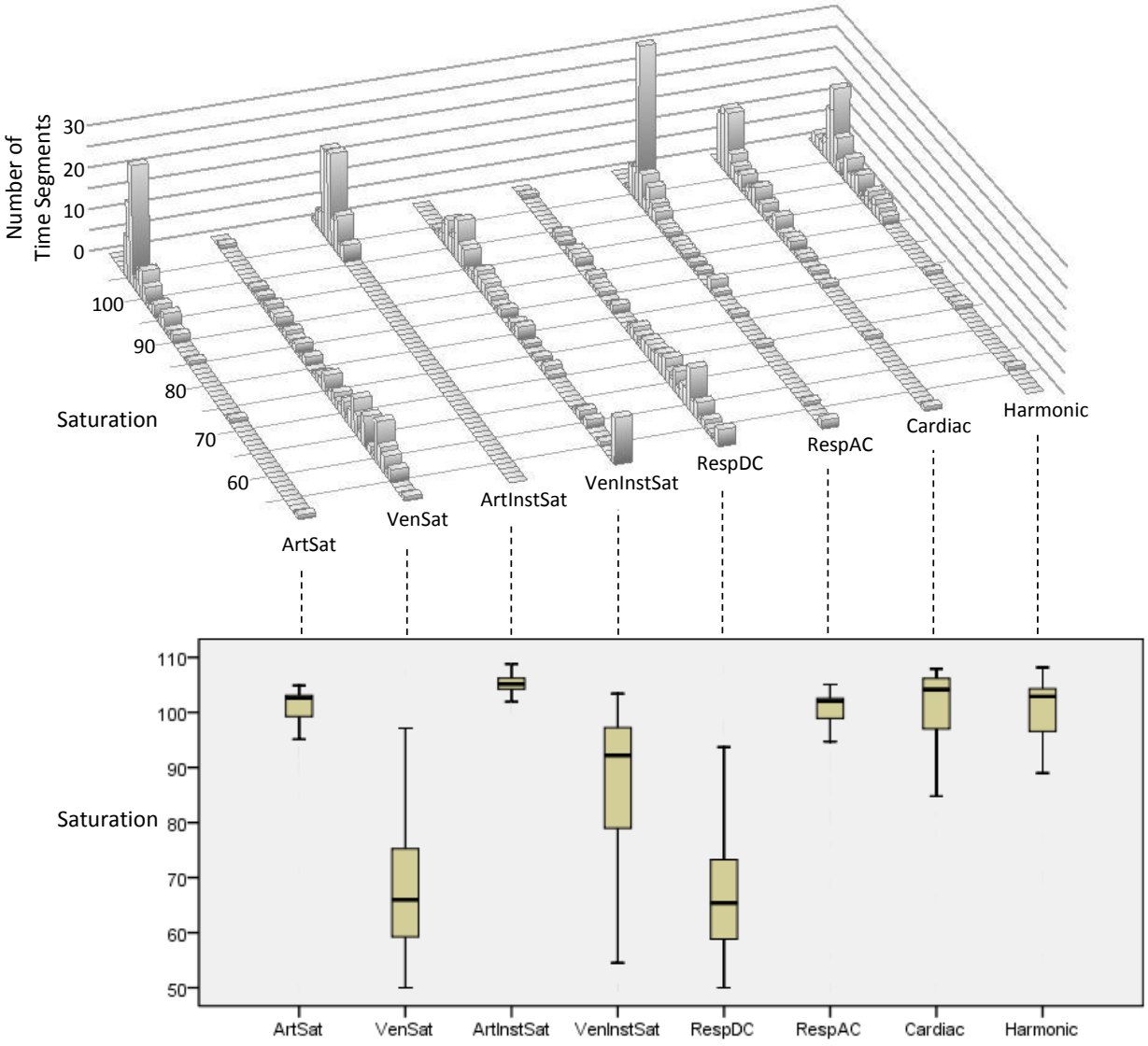

Figure C1 Histogram and box-and-whisker plot summarizing record for Patient 1 (C11). For each minute of data, the eight methods of calculating oxygen saturation are used to generate eight values of oxygen saturation. The distribution of values for a given saturation algorithm is illustrated by the histogram at the top of the figure, and by the corresponding box-and-whisker plots at the bottom of the figure. For a given saturation algorithm, the box-and-whisker plot contains a thin vertical line which signifies the upper and lower saturation values among the ten patients. The shaded bar extends from the 25^{th} quartile to the 75^{th} quartile. The horizontal line within the shaded bar corresponds to the median saturation.

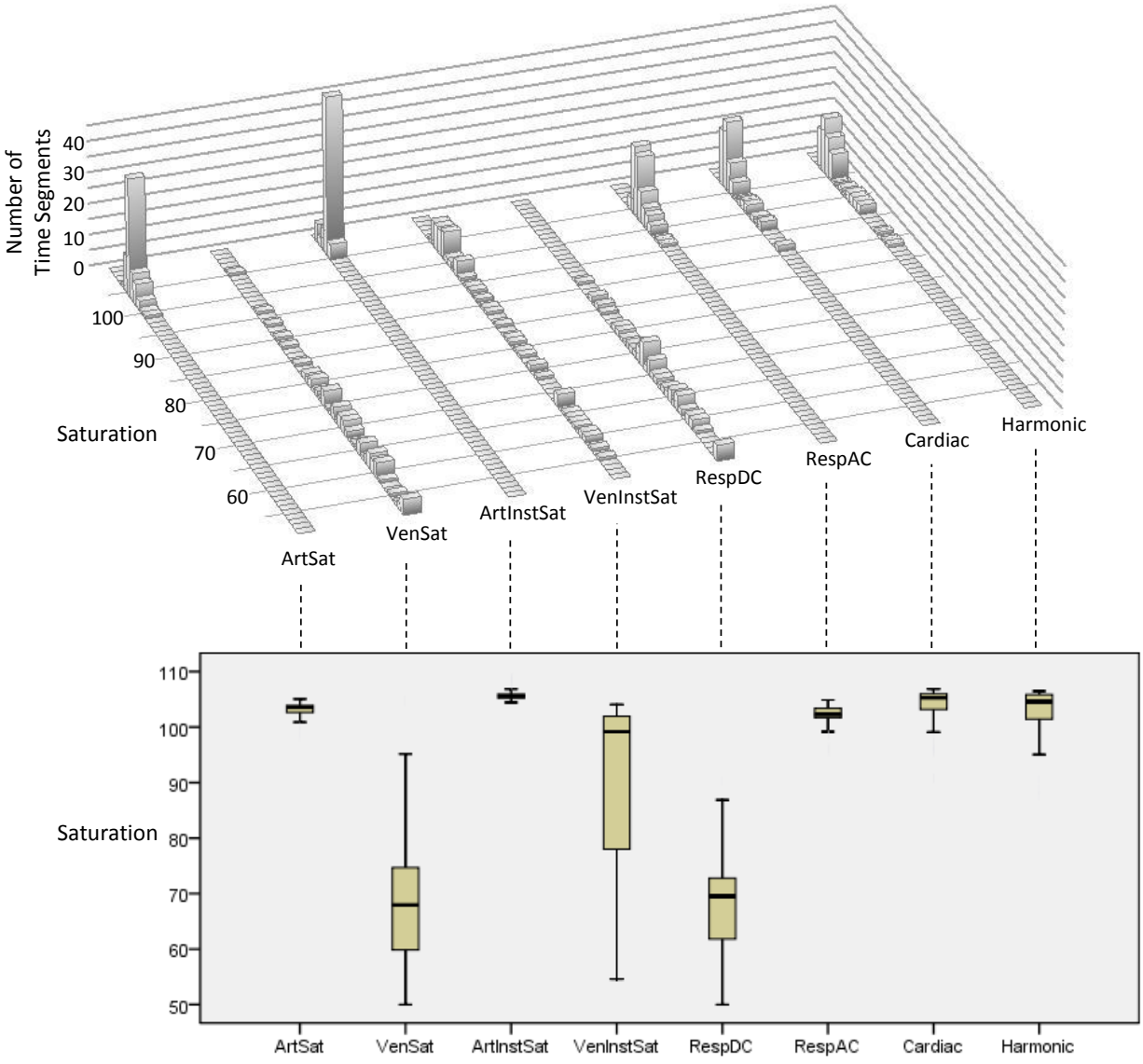

Figure C2 Histogram and box-and-whisker plot summarizing record for Patient 2 (C12). See the caption of Fig. C1 for an explanation of how these figures are generated.

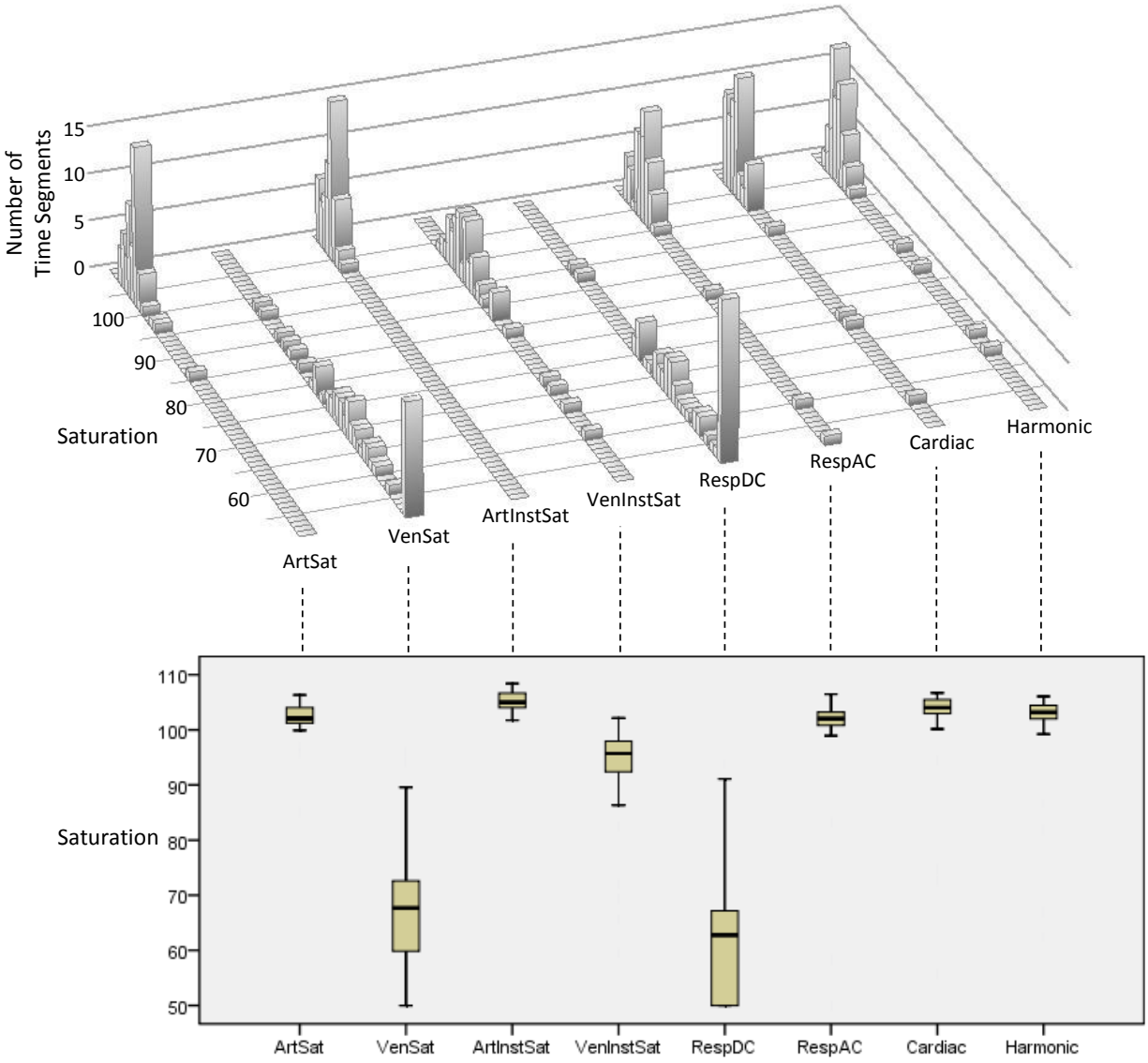

Figure C3 Histogram and box-and-whisker plot summarizing record for Patient 3 (C13). See the caption of Fig. C1 for an explanation of how these figures are generated.

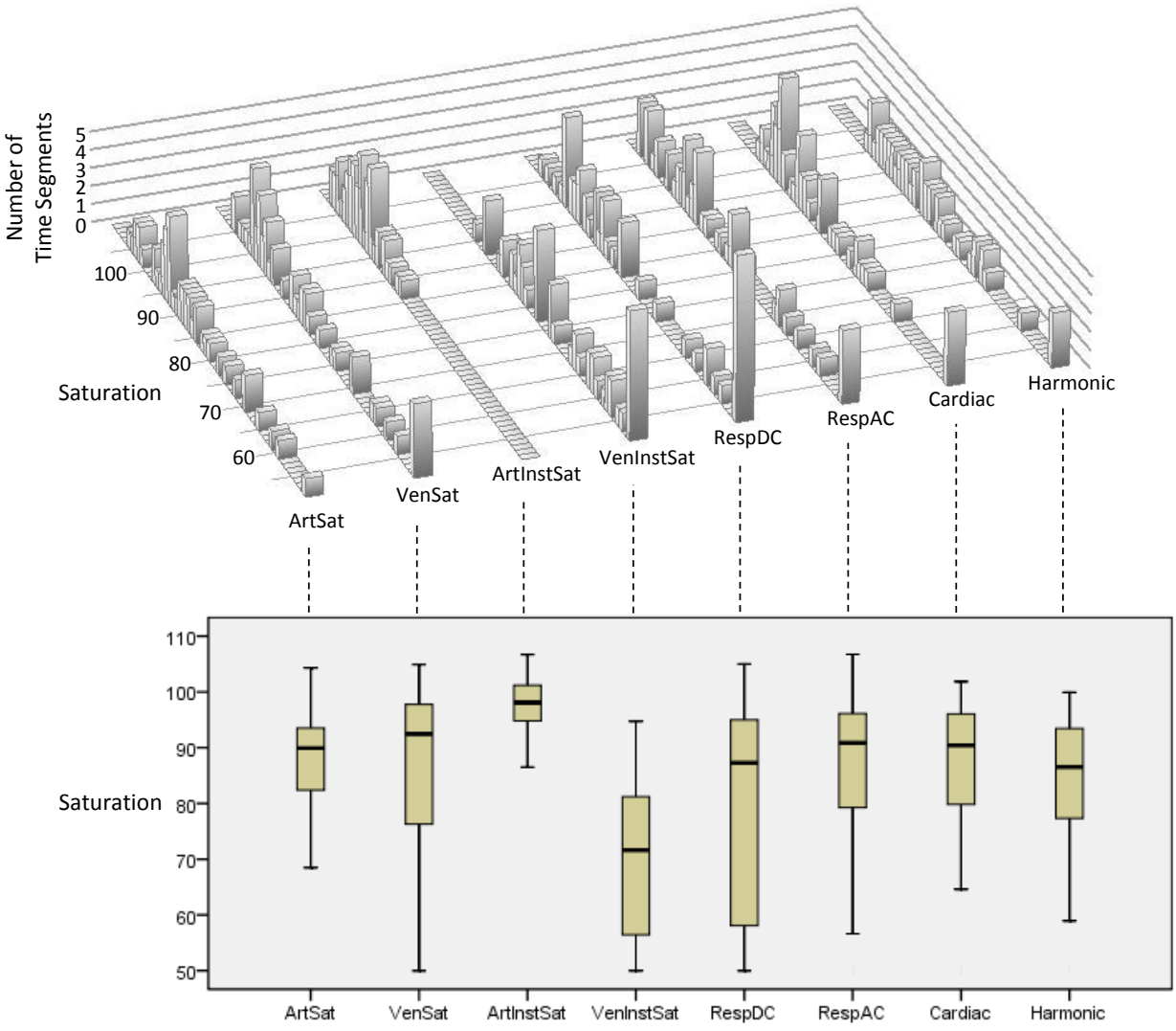

Figure C4 Histogram and box-and-whisker plot summarizing record for Patient 4 (C15). See the caption of Fig. C1 for an explanation of how these figures are generated.

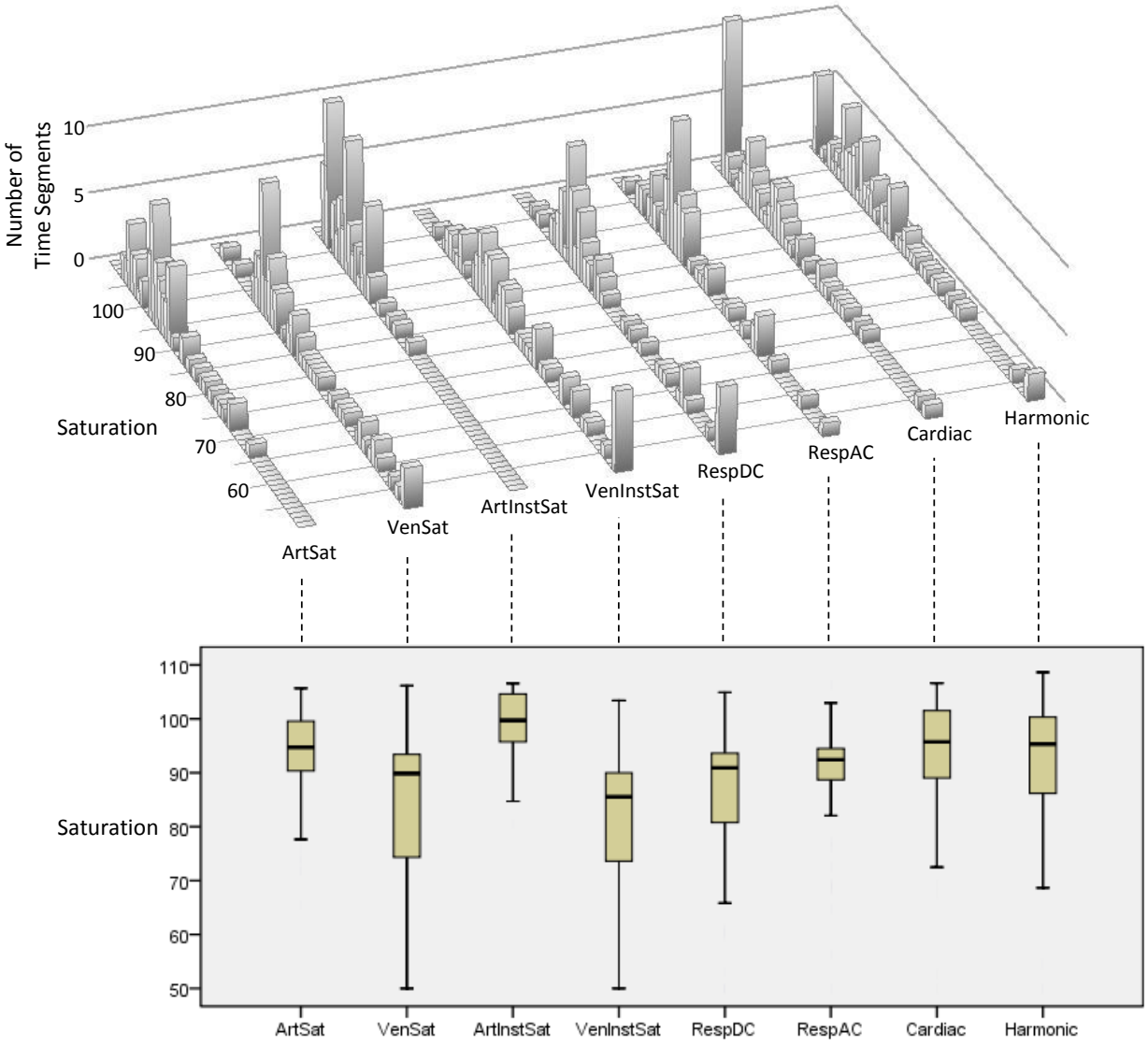

Figure C5 Histogram and box-and-whisker plot summarizing record for Patient 5 (C16). See the caption of Fig. C1 for an explanation of how these figures are generated.

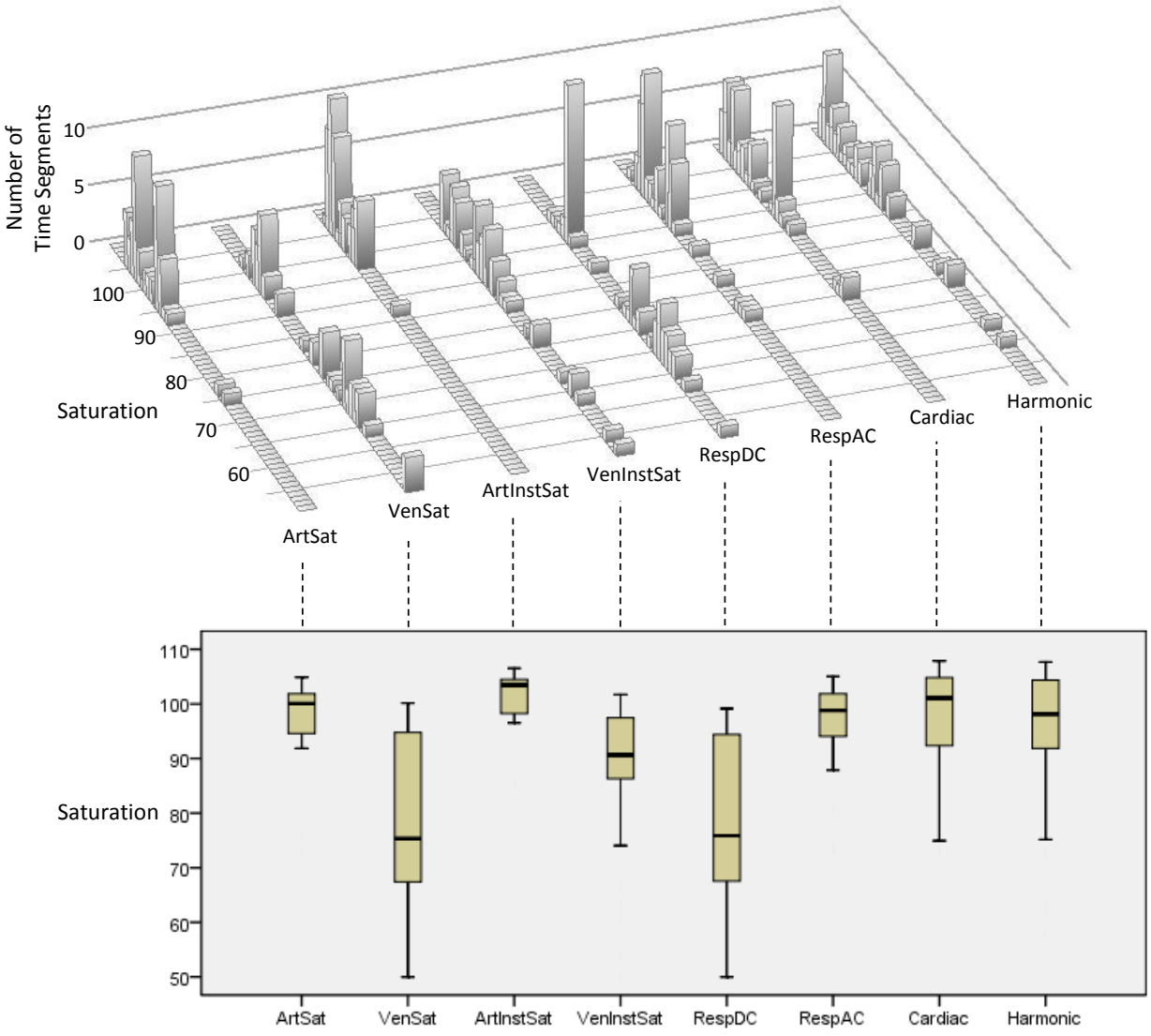

Figure C6 Histogram and box-and-whisker plot summarizing record for Patient 6 (C17). See the caption of Fig. C1 for an explanation of how these figures are generated.

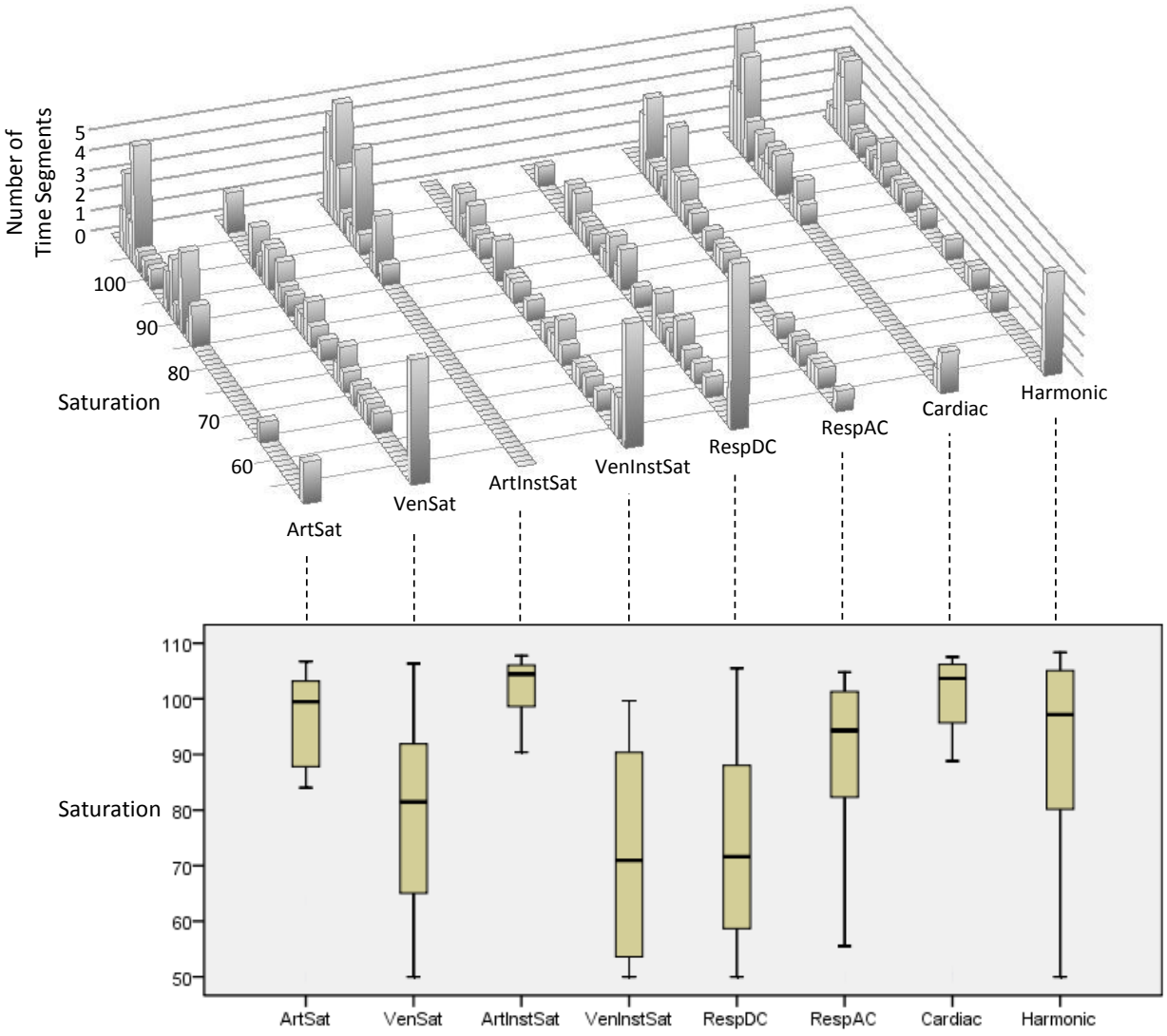

Figure C7 Histogram and box-and-whisker plot summarizing record for Patient 7 (C19). See the caption of Fig. C1 for an explanation of how these figures are generated.

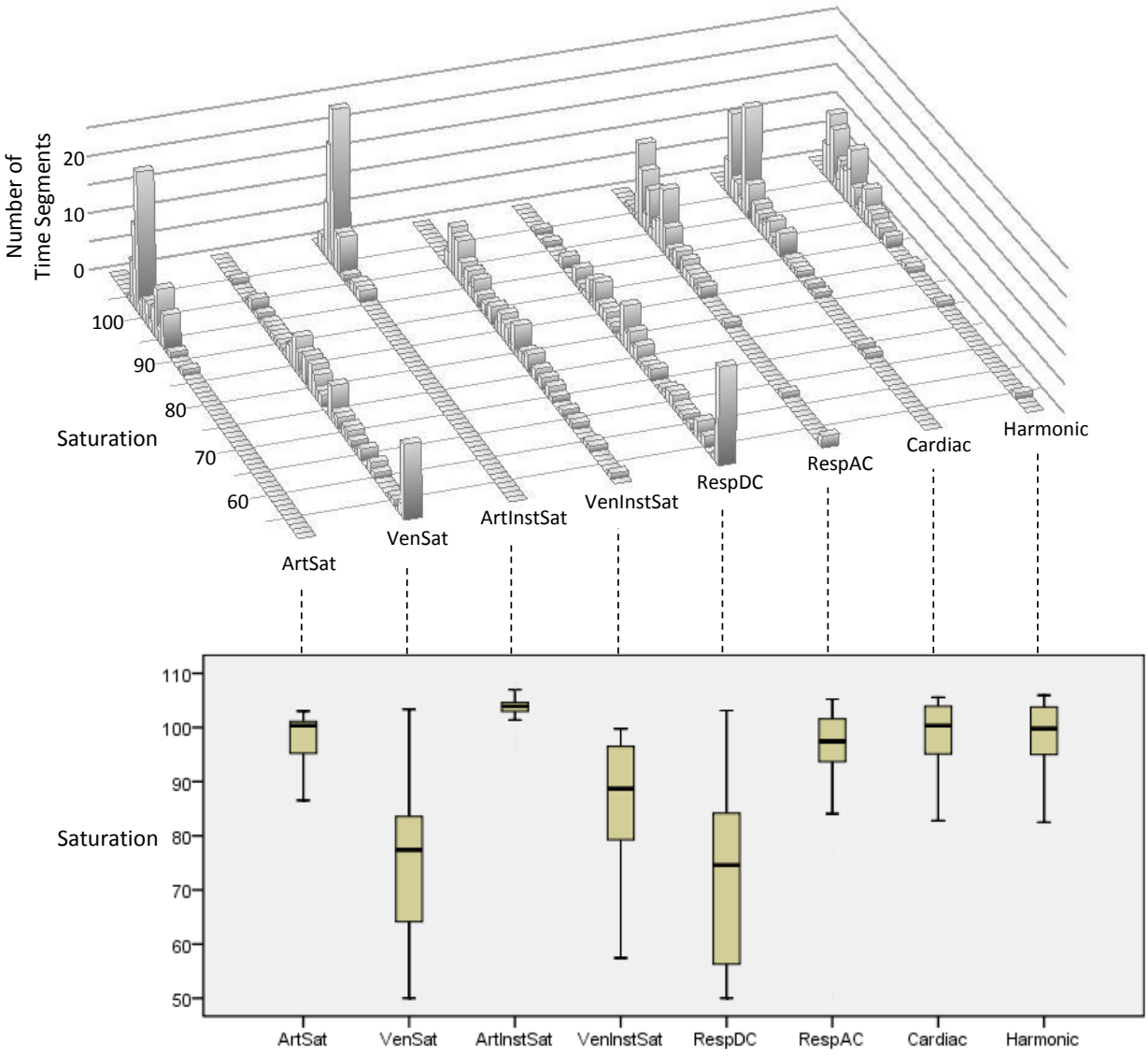

Figure C8 Histogram and box-and-whisker plot summarizing record for Patient 8 (C20). See the caption of Fig. C1 for an explanation of how these figures are generated.

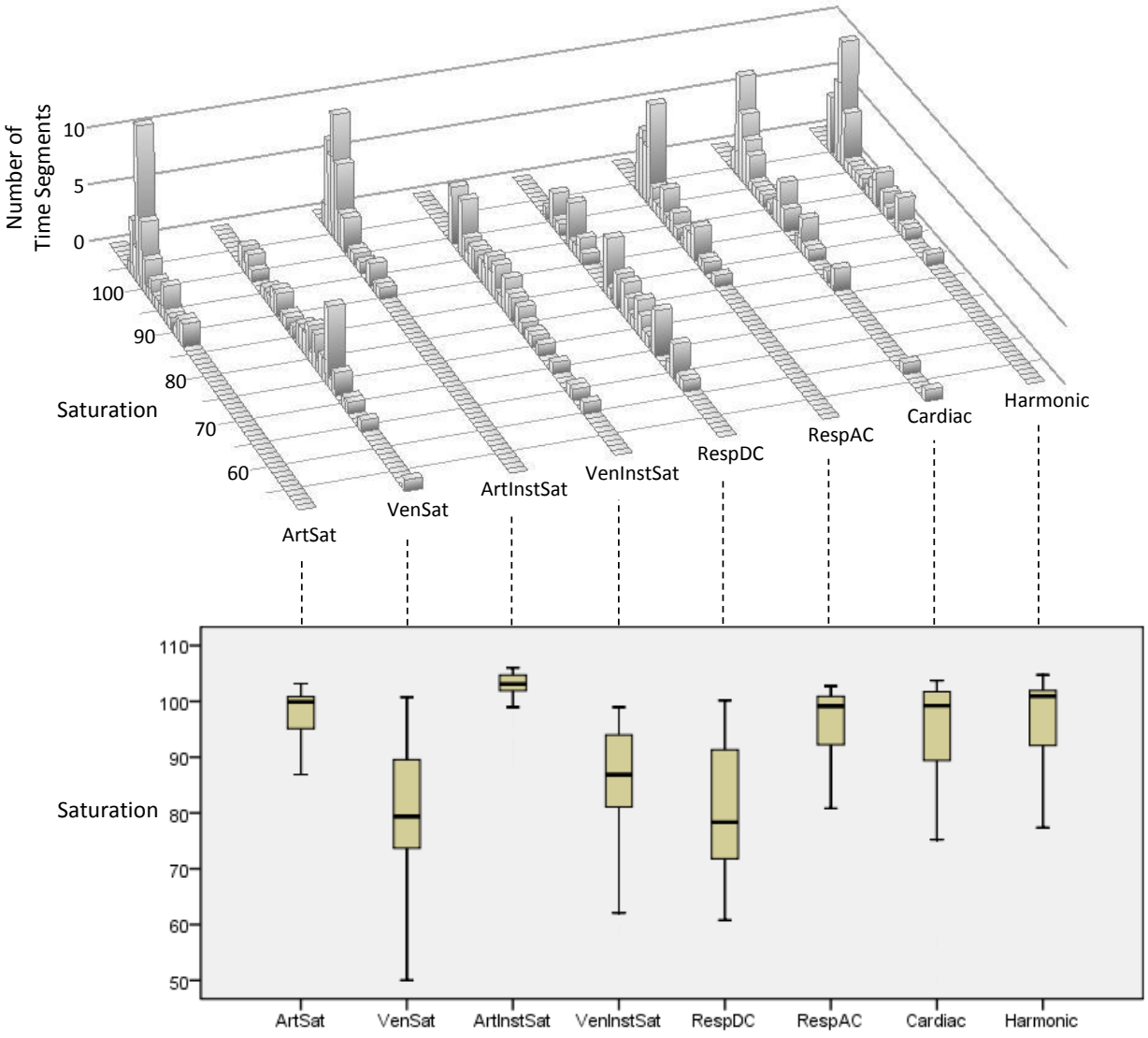

Figure C9 Histogram and box-and-whisker plot summarizing record for Patient 9 (C21). See the caption of Fig. C1 for an explanation of how these figures are generated.

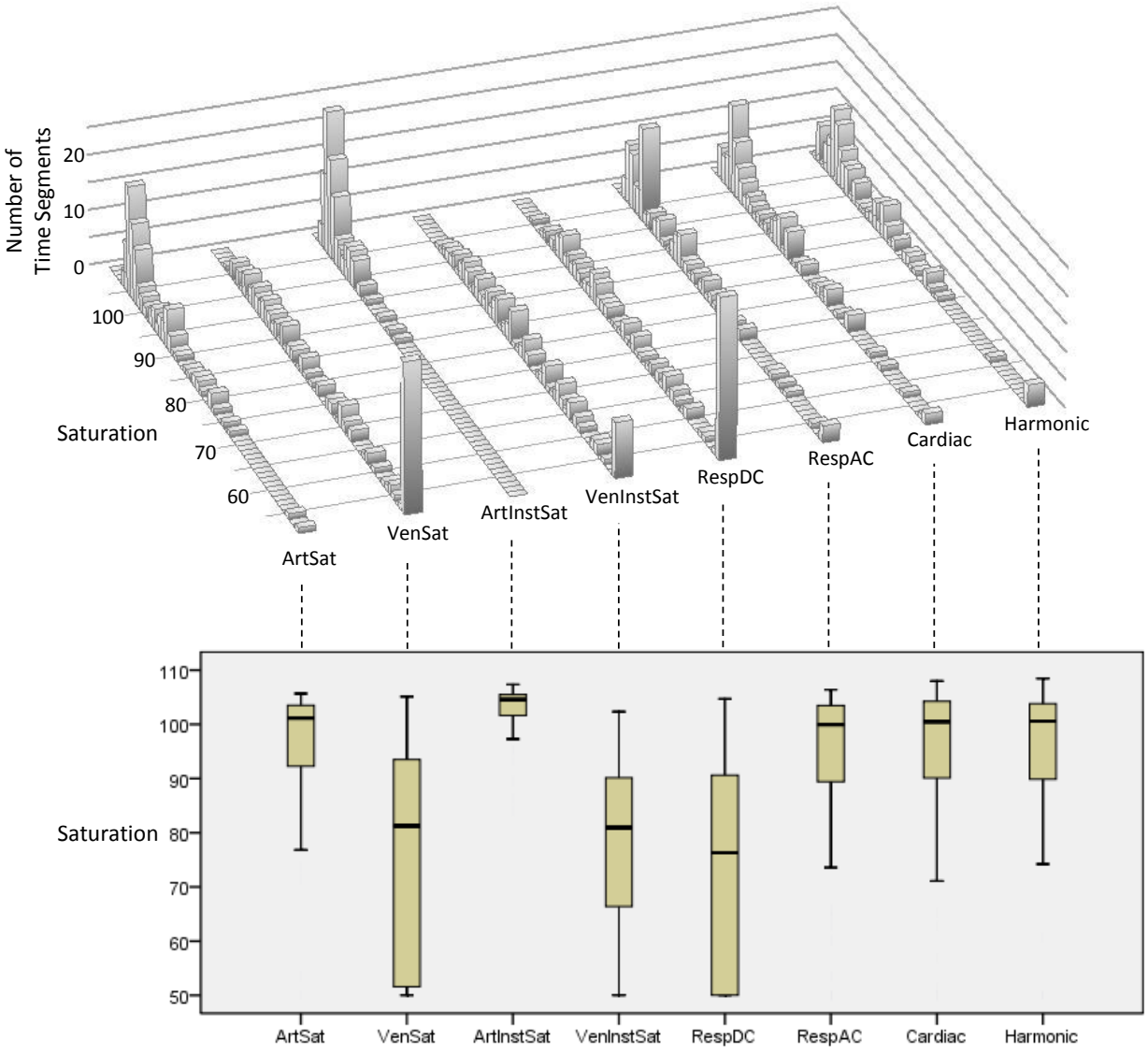

Figure C10 Histogram and box-and-whisker plot summarizing record for Patient 10 (C22). See the caption of Fig. C1 for an explanation of how these figures are generated.

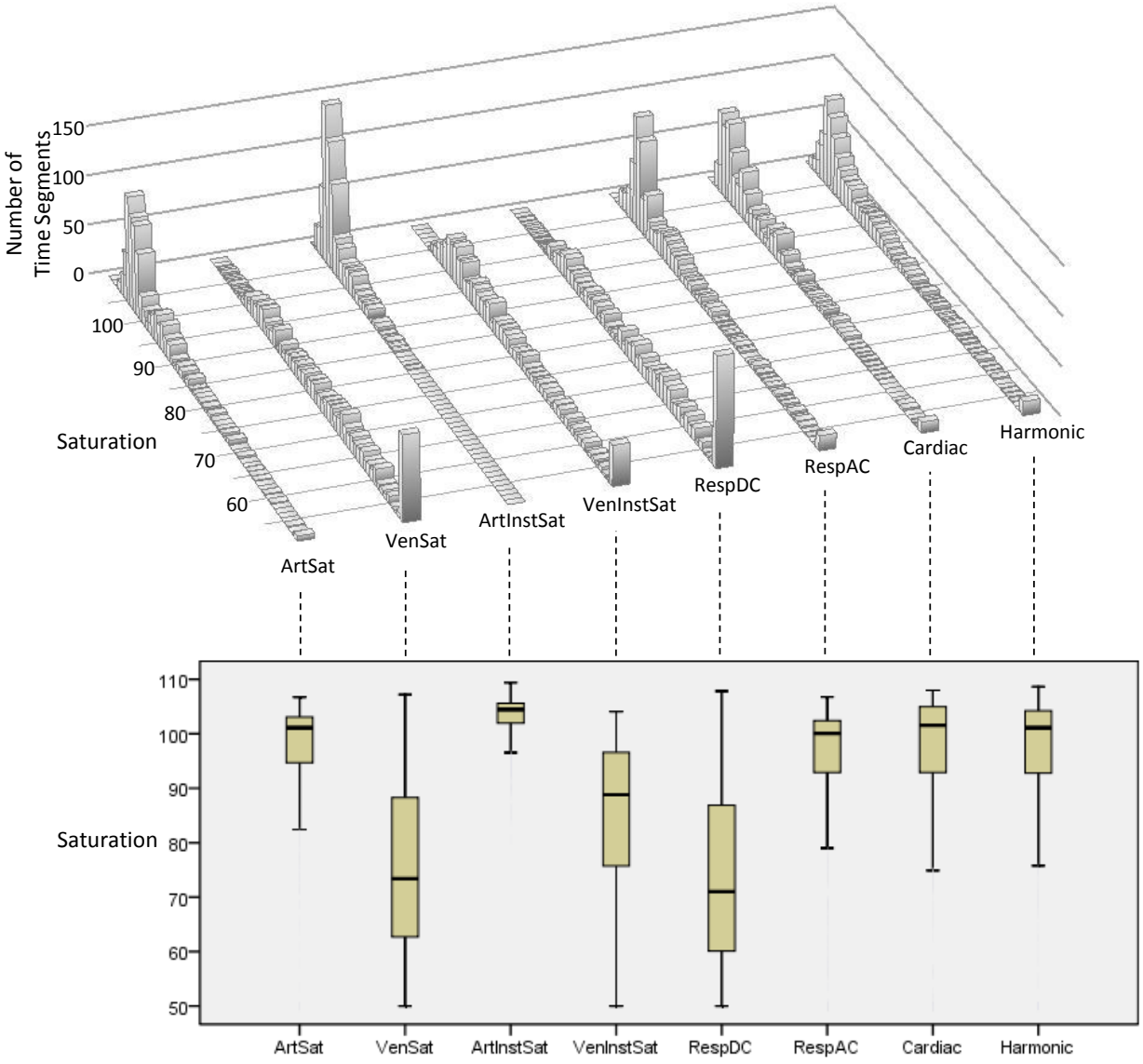

Figure C11 Histogram and box-and-whisker plot summarizing record for all ten patients combined. See the caption of Fig. C1 for an explanation of how these figures are generated..